UNIVERSITÀ DEGLI STUDI DI MILANO
FACOLTÀ DI SCIENZE MATEMATICHE,
FISICHE E NATURALI

Corso di Laurea Triennale in Fisica

Tesi di Laurea in Fisica

The Weinberg angle from the lepton Forward-Backward Asymmetry at the LHC

Relatore interno: Prof. S. Forte

Correlatore: Dott. A. Vicini

Relatore esterno: Dott. J. Rojo

Luca Rottoli
matr. 740309

Anno Accademico 2010/2011

Contents

1 Introduction **iii**

2 The Standard Model **1**
2.1 Physics of the weak interactions . . . 1
2.1.1 Parity violation and the V-A theory . . . 2
2.1.2 Gauge theory of the weak interactions . . . 3
2.2 The electroweak unification and $\sin^2\theta_W$ . . . 4
2.3 Strong interaction physics . . . 4
2.3.1 Structure functions and Bjorken scaling . . . 5
2.3.2 Quarks and gluons . . . 6
2.4 Quantum chromodynamics . . . 7
2.5 Factorization . . . 8

3 The Forward-Backward Asymmetry **9**
3.1 The Drell-Yan process . . . 9
3.2 The electroweak partonic process . . . 10
3.3 Parton distributions . . . 13
3.3.1 The "standard" approach: MSTW and CT10 . . . 13
3.3.2 The Monte Carlo approach: NNPDF . . . 14

4 Results **17**
4.1 Introduction . . . 17
4.2 Generation of events and settings . . . 17
4.3 A_{FB} sensitivity to the weak mixing angle . . . 18
4.4 PDF and statistical uncertainties on A_{FB} . . . 20
4.4.1 ATLAS/CMS kinematics . . . 21
4.4.2 LHCb kinematics . . . 27
4.5 PDF uncertainties by template fitting method . . . 35
4.5.1 General strategy . . . 35
4.5.2 Numerical Results . . . 35
4.6 Statistical uncertainties . . . 36
4.6.1 General strategy . . . 36
4.6.2 Results . . . 37
4.7 Summary . . . 42

5 Conclusions **43**

List of Tables **45**

List of Figures **46**

References **48**

Chapter 1

Introduction

The Standard Model describes completely three of the known basic interactions of nature and it is one of the greatest scientific achievement in the second half of the XX century. Various arguments however suggest that new physics beyond the Standard Model may be required. It is thus important to carefully verify the coherence of the Standard Model by stringent tests in order to uncover possible unknown physics. In this perspective precisions measurements at high energy colliders like LHC become crucial.

Electroweak unification is one of the cornerstones of the Standard Model and predicts the existence of a symmetry between the electric and the weak interactions which holds at high energy. The strengths of the fields are related by an arbitrary constant, the Weinberg angle denoted by $\sin^2\theta_W$. This parameter is known very accurately, but since there exists a certain tension between different fits it would be of great interest to perform a measurement with a smaller uncertainty.

The lepton Forward-Backward Asymmetry (A_{FB}) at the LHC is sensitive to the weak mixing angle. Hence from the measurement of this asymmetry it may be possible to obtain a precise measurement of $\sin^2\theta_W$. However, systematic uncertainties need to be sufficiently small in order to measure $\sin^2\theta_W$ at the desired level of accuracy. The main source of systematic errors in a hadron collider is the uncertainty which affects the parton distribution functions (PDFs), which limits the accuracy of our knowledge of proton structure.

In this thesis we study the impact of PDF uncertainties on a possible future measurement of $\sin^2\theta_W$ at the LHC studying A_{FB} as a function of the invariant mass of the lepton pair in Drell-Yan neutral current events. We have generated events using the event generator HORACE, and we have limited our study at the Born level. We have estimated the PDF uncertainties by means of a template fitting method, and we have combined the results with our estimate of the statistical uncertainty with an integrated luminosities of 100 fb^{-1}.

The thesis is organized as follows. In Chapter 2 we briefly give an overview of the Standard Model. In particular, we focus on the electroweak unification and on quantum chromodynamics (QCD). In Chapter 3 we study the Forward-Backward Asymmetry and its relation to the weak mixing angle. We describe the electroweak partonic process and we present the basic approaches on the determination of PDFs and their uncertainties. Finally, in Chapter 4 we study the PDF and the statistical uncertainties on A_{FB} and we estimate the impact of the uncertainties on the measurement of the weak mixing angle We draw our conclusions in Chapter 5.

Chapter 2

The Standard Model

The so called Standard Model, formulated in the 1970s, explains practically all experimental data from high energy physics experiments. According to this theory, a small number of fermions, six quarks and six leptons, can construct all of matter. The Standard Model also incorporates their interactions, which are explained in terms of gauge bosons exchanged between the fermion constituents. The gluon, a massless boson, is the particle mediating the interquark force which binds the quarks into the nucleons. Another massless boson, the photon, mediates the electromagnetic interactions. The weak interactions, responsible for the nuclear β-decays, are mediated by three bosons, $W^{\pm}$ and Z^0, which have masses two order of magnitude bigger than the proton mass.

The Standard Model thus provides a theory which describes three of the known basic fields of nature, but it is still subjected to limitations. Gravitational interactions, putatively mediated by a spin 2 boson, the graviton, are not included in the Standard Model, and the attempts performed in order to include gravity, despite the efforts, have made little progress. Moreover, though in the simplest version of the Standard Model the neutrinos are massless, anomalies in the Standard Solar Model opened out to the hypothesis of neutrino oscillations and experiments show that neutrinos do have finite masses. Cosmological observations will require new and unknown physics beyond the Standard Model in order to explain the existence of dark matter and dark energy. Finally, it is yet unclear where the number of free parameters needed by the theory comes from.

Precisions measurements at high energy colliders such as LHC are extremely important in order to test the Standard Model and eventually to discover new physics behind it.

2.1 Physics of the weak interactions

The first descriptions of the weak interactions was formulated by E. Fermi in 1934. He described β decay as an interaction between two currents, the former converting a neutron in a proton and the latter creating an electron and its antineutrino. Fermi hypothesized a contact interaction. The four fermions were thought to interact in a single point: the wave functions of neutron and neutrino (equivalent to the outgoing antineutrino) transformed into the wave functions of the proton and the electron. In this description the matrix element for the β decay can be written

as

$$M \propto (\bar{\psi}_p \Gamma \psi_n)(\bar{\psi}_e \Gamma \psi_\nu), \tag{2.1}$$

where the Γ factors (matrices, in general) contain the quantum numbers of weak interactions. The nature of these factors was explained years later, when it was discovered that weak force violates parity.

The theory of a point-like interaction, unfortunately, leads to wrong predictions when applied to high-energy weak interactions. It is thus necessary to replace the theory of contact interaction with a theory based on a particle-exchange mechanism. The particle which carries that interaction is an intermediate vector boson and it is denoted W, and must be very massive as the range of the force is very short. The two currents involved in a weak interaction now couple to the W boson, which mediates the interaction between different space-time points. The W boson must come in two oppositely charged versions, as in the interactions it couples to particles which have different charge. In order to include neutral currents phenomena, we must take into account the existence of a neutral boson.

2.1.1 Parity violation and the V-A theory

The solution of the $\theta - \tau$ puzzle in the 1950s led to the conclusion that the force responsible for the decay does not conserve parity. Lee and Yang examined the experimental informations which concerned this problem and pointed out that there was no evidence either of conservation or nonconservation of parity in weak interactions. Further experiments aimed at testing evidences of violation of parity in other weak processes, and finally C. S. Wu and others observed a large asymmetry in the decay of ^{60}Co. The mirror process thus behaves differently from its real image and the weak force can distinguish a left-handed from a right-handed coordinate system.

In 1957 Feynman and Gell-Mann proposed the so called V-A theory, a modification of the Fermi theory of weak interactions, in order to take into account the recent experimental results. They considered the matrix element (2.1) and showed that if the interaction factor Γ is a mixture of vector and axial-vector quantities, and thus if there are a vector (V) and axial-vector (A) current in the interaction, it is possible to explain the parity violation by the weak force. In fact vectors and axial-vectors behave differently under parity. The vector changes sign under parity transformation, but the axial-vector does not: thus if the interaction is characterized by both the components it will be non-invariant under parity.

The choice of such interaction factors has also another relevant consequence. In fact, weak interactions couples to fermions in a peculiar way. When the fermions move close to the speed of light c it is convenient to classify fermion states in a new way. Define the helicity as

$$H = \frac{\sigma \cdot \mathbf{p}}{|\mathbf{p}|}, \tag{2.2}$$

where $\mathbf{p}$ is the momentum of the particle. The fermion can thus be in the helicity-plus or in the helicity-minus state, depending on the fact that the spin is aligned or not with the momentum. In case of massless particle, helicity is a well-defined, Lorentz-invariant quantity, while for massive particles it is not invariant under Lorentz transformations. Then it is useful to make a further classification, called chirality or handedness (which coincide with helicity for massless particles). The eigenstates of chirality have the important property that they are interchanged under parity:

left-handed (helicity-minus) states become right-handed (helicity-plus) states and conversely. Weak charged currents, which violate parity, have the important property of coupling uniquely to left-handed fermions (and right-handed antifermions) only.

2.1.2 Gauge theory of the weak interactions

Gauge invariance is one of the most important concept in modern physics and it applies to all the four fundamental forces of nature. In a gauge theory we must ensure that the Lagrangian which describes interactions remains invariant under symmetry transformations performed by an appropriate symmetry operator. Additional fields must be introduced in order to get a local symmetry and this lead to the introduction of definite physical forces.

The first gauge theory which has been formalized was QED, which attempts to describe the interaction of charged particles, in such a way that total electric charge is always conserved. The gauge invariance of Maxwell's equations is related, in the quantum form of the theory, to an invariance under local transformation of the quantum fields. The demand of a certain type of phase invariance of the electron wave function dictates the form of the interaction: this is the basis of the gauge principle.

QED is characterized by another crucial property: renormalizability. Higher-order terms in perturbation theory involve integrals over the four-momenta of intermediate virtual particles. Those integrals are often formally divergent, and it necessary to impose some form of cut-off procedure. If divergences can be absorbed in the definition of a finite number of parameters (such as masses and couplings), the theory is said to be renormalizable. From renormalization procedure an crucial fact emerges: the coupling constants, such as α, are not actually constant but vary logarithmically on the energy scale at which measurements are made. We will develop this last observation further in the section dedicated to strong interaction physics.

Also weak interactions can be described as a gauge theory. Since weak interactions do not depend on the charge of particles, they must be independent of the electrical charge of the particles experiencing its action. It is then possible to define a weak isospin in analogy with the isospin of nucleons and then to require the Lagrangian invariance under the group of weak isospin rotations, $SU(2)^W$. Furthermore, we demand invariance of the Lagrangian under local gauge transformation. This can be obtained introducing a field A^α_ν, which is interpreted as the boson, such that

$$\mathbf{G}^{SU(2)^W}(x)\mathcal{L}(l_e, l_\mu, A^\alpha_\nu) \rightarrow \mathcal{L}(l^*_e, l^*_\mu, A^{\alpha *}_\nu), \tag{2.3}$$

where we have denoted as l_e and l_μ the doublets

$$l_e = \begin{pmatrix} \nu_e \\ e^- \end{pmatrix}, \qquad l_\mu = \begin{pmatrix} \nu_\mu \\ \mu^- \end{pmatrix}. \tag{2.4}$$

This leads to two important consequences: the gauge field coincides with a charge triplets and, moreover, the gauge bosons must be massless.

Apparently, the request of renormalizability implies the masslessness of gauge bosons. Massive vector fields are not gauge invariant and not renormalizable. However, a mechanism (the so called Higgs mechanism) to endow gauge bosons with mass without breaking gauge invariance was discovered in 1964. It was already proved in the early 1960s that whenever a global symmetry is spontaneously broken a massless, spin 0 particle results (the Goldstone boson). Nevertheless,

if the symmetry which is broken spontaneously is local, a mass for the gauge bosons may be generated without altering the number of degrees of freedom of the system. It is thus possible to start with a gauge-invariant theory and let gauge bosons acquire mass.

The Higgs mechanism implies the existence of a massive spin-0 particle, known as Higgs boson, which has not been observed yet.

2.2 The electroweak unification and $\sin^2\theta_W$

Early theories of weak interactions did involved divergences at high order, that could be cancelled only by introducing an increasing number of constants. The Standard Model incorporates the Higgs mechanism to generate the masses of the W boson. Between 1967 and 1968 S. Glashow, A. Salam and S. Weinberg independently formulated the principles of the Electroweak unification, one of the cornerstones of the Standard Model. They predicted that there exists a symmetry between electric and weak interactions at very high momentum transfer ($q^2 \gg 10^4$ GeV^2) and that at low energy the symmetry would be broken: of the four mediating vector bosons involved, one would be massless (the photon) and the others, namely W^+, W^- and Z, would become massive. As a result, at low energy weak interaction are feeble and short-ranged, if compared with electromagnetic interaction. The theory contains an arbitrary constant, the weak mixing angle or Weinberg angle denoted by $\sin^2\theta_W$, which relates the strengths of the electromagnetic and the weak interactions.

This constant is necessary because it turns out that the particle which remains massless - the photon - must be a linear combination of two gauge bosons of the underlying fundamental theory. This is necessary in order to reconcile the fact that matter particles which are degenerate under the weak interactions have a different electric charge, with the desire to preserve simultaneously gauge invariance of the weak and electromagnetic interactions.

Once gauge bosons acquire mass through the Higgs mechanism, their masses and the electroweak mixing angle become related, according to the following equation:

$$\sin^2\theta_W = 1 - \frac{M_W^2}{M_Z^2}. \tag{2.5}$$

This relation holds at the lowest perturbative order, and it gets modified by radiative corrections.

It can be demonstrated that the weak neutral current can be written as [8]:

$$J_\mu^0 = 2J_\mu^3 - 2\sin^2\theta_W J_\mu^{EM}, \tag{2.6}$$

where J_μ^3 is the third component of the weak isospin current and J_μ^{EM} is the electromagnetic current. Thus experiments involving neutral currents can be performed in order to evaluate $\sin^2\theta_W$.

2.3 Strong interaction physics

In the last decades scattering experiments have been the primary source of information on the structure of nucleons. Beams of energetic leptons (usually electrons) are made to collide with hadrons and the results of the collision, which is mediated by the electromagnetic interaction, are collected by detectors. Elastic scattering experiments in the 1950s and in the 1960s suggested

that the nucleons do not have a point-like structure. In order to resolve the nucleon structure it was thus necessary to increase the energy of the probing beam. In this way the wavelenght of the exchanged photon is smaller of the size of the target. As the transferred momentum of the photon increases, deep inelastic scattering (DIS) arises: the nucleon disintegrates and new particles are produced.

2.3.1 Structure functions and Bjorken scaling

The main measurement of scattering experiments is the variation of the cross-section with the scattering angle and the final energy of the lepton. However, other kinematics variables may be used and it becomes natural to study the variation of the cross-section with the transferred energy ν and the square of momentum transferred by the photon $Q^2 = -q^2$.

If one assumes that the electromagnetic interaction between the electrons and the nucleon is dominated by single photon exchange, it is possible to obtain a rather simple mathematical description of a scattering experiment. QED provides a tool to calculate the lepton current and the propagation factor associated to the photon, but it is impossible to describe the structure of the nucleon using perturbative methods. It is then necessary to introduce a number of structure functions which are determined by experiment. It is possible to demonstrate that the differential cross-section for electron-nucleon scattering can be written as

$$\frac{d^2\sigma}{dQ^2 d\nu} = \frac{4\pi\alpha^2}{Q^4}\frac{1}{M}\frac{E_f}{E_i}\left[\frac{M}{\nu}F_2(Q^2,\nu)\cos^2\frac{\theta}{2} + 2F_1(Q^2,\nu)\sin^2\frac{\theta}{2}\right]. \tag{2.7}$$

At the beginning, the main goal of DIS experiments was to study the resonance production which characterizes the cross-section once θ is fixed. However the data show that as the transferred momentum increases, the cross-section becomes independent from Q^2. J. Bjorken interpreted these asymptotic behaviour and hypothesized that in the limit $Q^2, \nu \to \infty$, and for finite value of the ratio

$$x = \frac{Q^2}{2M\nu}, \tag{2.8}$$

the structure functions would depend only on that dimensionless ratio:

$$F_{1,2}(Q^2,\nu) \overset{Q^2,\nu\to\infty}{\longrightarrow} F_{1,2}(x). \tag{2.9}$$

A first interpretation of this phenomenon was given in a model proposed by R. P. Feynman, which is known as *parton model*. He proposed that the nucleon is made up of partons, smaller point-like and non-interacting constituents. The structure functions measure the way in which the nucleon momentum is distributed between the partons.

It is possible to obtain important relations between the structure functions and the properties of partons comparing the cross-section in Eq. (2.7) to the cross-section describing the interaction between an electron and a point-like fermion. In order to perform such a comparison, we hypothesize that each parton has a charge e_i and has a probability $\frac{dP}{d\beta} = f_i(\beta)$ of carrying a fraction β of the total momentum of the nucleon. Finally, the total momentum carried by the partons must be equal to that of the nucleon. Such a relation can be written as

$$\sum_i \int_0^1 dx\ x f_i(x) = 1, \tag{2.10}$$

where the sum runs over all the partons. The cross-section may finally be calculated as the incoherent sum of the interactions between the photon and the single partons.

Comparing the results, it is possible to relate the structure functions to the individual parton distribution, obtaining:

$$F_1(x) = \sum_i f_i(x) e_i^2, \tag{2.11}$$

$$F_2(x) = x \sum_i f_i(x) e_i^2. \tag{2.12}$$

The functions $f_i(x)$, which must be experimentally determined, are known as parton distribution functions (PDF).

2.3.2 Quarks and gluons

One of the important relation which can be obtained comparing QED cross-section describing electron-fermion scattering and the cross-section Eq. (2.7) relates the structure functions in a simple way:

$$2xF_1(x) = F_2(x). \tag{2.13}$$

If the ratio $\frac{2xF_1(x)}{F_2(x)}$ is experimentally equal to one, this provides evidence for the fact that partons are spin $\frac{1}{2}$ particles, and this is indeed the case. It was then natural to compare the parton model to the *quark model*, introduced in 1964 by M. Gell-Mann and G. Zweig. The quark model explained brilliantly the variety of hadrons hypothesizing that they can be classified if organized in a SU(3) symmetry scheme. However, the model introduced new physical entities, which Gell-Mann baptized *quarks*, with fractional barion number and fractional charge. It seemed unlikely that nucleons were characterized by internal structure, and the model was perceived more likely as a mathematical tool than a theoretical explanations of the hadron structure. The success of the parton model urged the scientific community to seriously reconsider Gell-Mann's hypothesis.

It is possible to compare the predictions of the Gell-Mann model to the parton model. As in the quark model the proton is a bound state *uud*, the following constraints are implied:

$$\int_0^1 dx\ (f_u(x) - f_{\bar{u}}(x)) = 2, \qquad \int_0^1 dx\ (f_d(x) - f_{\bar{d}}(x)) = 1. \tag{2.14}$$

The integration over the quark momentum distribution gives the fraction of the momentum that the quark carries:

$$P_u = \int_0^1 dx\ x(f_u(x) - f_{\bar{u}}(x)). \tag{2.15}$$

Measurements confirm indeed these expectations. However, experiment shows that the total fractional momentum carried by quarks is about one-half of the total proton momentum. We interpret this fact assuming that the remaining half is carried by neutral gluons, the quanta of the strong nuclear force which do not experience electromagnetic force.

2.4 Quantum chromodynamics

The parton model today is viewed as an approximate consequence of the leading order perturbative treatment of QCD, the modern theory of strong interactions. While a full treatment of QCD is beyond the scope of this thesis, it will be sufficient to state that QCD is, like QED and electroweak theory, a gauge theory, based on the gauge group $SU(3)$, conventionally called color.

In this respect, QCD is very similar to QED, which describes electric charges as the sources of the electromagnetic field. Nevertheless, there are important differences between the two theories. A first difference involves the quanta of their respective fields. The photon in fact is neutral, and as a result it does not interact with itself. On the contrary, in QCD the $SU(3)$ gauge fields, the gluons, carry the color charge, and thus they are self-interacting.

In quantum field theories the intrinsic strength of a force, which is related to the coupling constants which characterize the interactions, depends on the energy scale. In the simpler case of the electromagnetic field, the strength of the interaction is fixed by the value of the fine structure constant α. The quantum mechanical effects which arises when the momentum transfer increases can be described as the creation of virtual electron-positron pairs from the vacuum. The cloud of virtual positrons shields the bare electron in the same way a dielectric is polarized by a test particle. Therefore the effective electric charge is appreciably reduced by the positive shield, and when the transferred momentum increases so does the fine structure constant. In fact the more the distance from the bare electron decreases, the more the virtual cloud is penetrated and the bare negative charge is less shielded.

A similar phenomenon exists in QCD, but the effect of color on a polarized medium is more complex. In fact gluons, which carry color charge, must be taken into account when the dependence of the strong coupling constant α_s from the energy scale is studied. The presence of gluon-shielding, due to the fact that gluons are self-interacting, provides an anti-screening effect. The effective color charge is bigger than the original bare charge. The strength of the strong interactions thus decreases with the transferred momentum, and vanishes asymptotically. The fact that at infinite energies quarks behave as free particles is known as *asymptotic freedom*. The limit of QCD for high-energy hadrons is consistent with the parton model, where observables are calculated as the incoherent sum of the interactions with the single partons.

Since the strength of coupling in QCD decreases at high energy, it is possible to calculate perturbatively the effect of color interactions. QCD predictions at large momentum scales are expected to be particularly accurate and can be experimentally checked.

On the other hand, at low energies the value of the coupling constant rises and thus it is not possible to perform perturbative calculations. Moreover, quarks can form bound states, which are the well-known hadrons. We have only a phenomenological knowledge of the nonperturbative QCD. When a bound $q\bar{q}$ pair is forced to separate, the potential between the quarks increases. At some separation length, it becomes convenient for the $q\bar{q}$ pair to split up in two $q\bar{q}$ pairs. The strong color attraction precludes the possibility of observing isolated quarks. This experimentally checked effect is known as *confinement*. This fact is observed whenever a high-energy collision takes place. The additional quarks or gluons produced in the collisions dress themselves into hadrons and form jets of particle which are seen in the detectors.

The strong nuclear force between hadrons can be thought as a residual-color Van der Waals force, which reflects the presence of a stronger interactions between the hadrons constituents. This interpretation is useful because it could be an intuitive explanation of the short-range

nature of the strong force between hadrons, as Wan der Waals interactions fall off more rapidly then the Coulomb force.

2.5 Factorization

One of the basic properties of QCD which makes it predictive in the perturbative regime is the factorization of cross-sections into hard cross-sections and universal parton distribution. Cross-sections for hard processes can be written as the convolution of a calculable parton interaction and the parton densities. In case of an hadroproduction processes we have:

$$\sigma_X(s, M_X^2) = \sum_{a,b} \int_{x_{\min}}^{1} dx_1 dx_2 f_{a/h_1}(x_1, M_X^2) f_{b/h_2}(x_2, M_X^2) \hat{\sigma}_{ab\to X}(x_1 x_2 s, M_X^2), \tag{2.16}$$

where $f_{a/h_i}(x_i)$ is the parton distribution function of partons of flavour a in the ith incoming hadron, and $\sigma_{ab\to X}$ is the parton level cross-section for the production of the final state X. The minimum value $x_{\min}$ is defined as $x_{\min} = \frac{M_x^2}{s}$.

While the parton distribution functions f_{a/h_i} are extracted from experiment, the cross-section in Eq. (2.16) can be expanded in perturbative series as to get at the desired level of accuracy:

$$\hat{\sigma}_{ab\to X}(x_1 x_2 s, M_X^2) = [\hat{\sigma}_0 + a\hat{\sigma}_1 + a^2\hat{\sigma}_2 + \ldots], \tag{2.17}$$

with $a = \frac{\alpha_s(M_W^2)}{2\pi}$. Eq. (2.16) is applicable to a wide variety of hard-scattering processes. Most processes have been calculated to the next-to-leading order (NLO) in perturbation theory, and thus up and including σ_1 terms.

The evolution of parton distributions $f_{a/h_1}(x_1, Q^2)$ at any scale is given by the Altarelli-Parisi (DGLAP) equations. They describe the Q^2 dependence of parton distributions, given their form at some reference scale Q_0. Qualitatively, these equations predict that partons tend to radiate forming new partons at lower x. Hence, parton distributions increase at small x and decrease at high x as Q^2 increases. As we probe hadrons deeper, it seems that they are formed by an increasing number of constituents. The more the momentum of the probe increases, the more the continual exchange of momentum between the nucleon constituent becomes appreciable. A consequence of perturbative QCD is thus that structure functions do not have a constant shape for all values of the transferred momentum. In QCD, Bjorken scaling is broken by logarithms of Q^2.

Chapter 3

The Forward-Backward Asymmetry

In the Standard Model neutral currents can be defined as a mixture of the third component of the weak isospin current and the electromagnetic current as in Eq. (2.6). Parity violating effects by weak currents lead to a charge asymmetry in the angular distribution of Z^0 decay [9]. This asymmetry depends on the relative strengths of the weak and electromagnetic currents, and thus it depends on $\sin^2\theta_W$.

At hadron colliders the study of the Z boson physics allows the determination the weak mixing angle through the measurement of the Forward-Backward Asymmetry in the neutral current channel of the Drell-Yan process.

The measurement of the Forward-Backward Asymmetry is traditionally a domain of e^+e^- collider experiment. At hadron colliders both practical and theoretical difficulties arise. Firstly, in pp collision the center of mass frame and the laboratory frame do not coincide, unlike in e^+e^- experiments and, moreover, the quark direction is unknown [10]. Secondly, systematical errors, from which PDF uncertainties are thought to play an important role, must be small in order to measure the weak mixing angle with the desired accuracy.

In this chapter we briefly present the Drell-Yan process in Section 3.1, we focus on the electroweak partonic process and its kinematics in Section 3.2 and we finally give an overview on the approaches used to determine the parton distribution functions and their uncertainties in Section 3.3.

3.1 The Drell-Yan process

In hadronic colliders, most collisions involve only soft interactions between the constituent quarks and gluons. It is impossible to treat such collisions with perturbative QCD. In some collisions, however, two quarks or gluons may exchange a large momentum $p_\perp$ perpendicular to the axis of collision. In this case, the elementary interactions take place very rapidly and it is possible to describe the process using perturbative theory. In case of a quark-antiquark scattering into a final state K, it is thus possible to consider a factorized cross section, which has the form

$$\sigma(p(P_1)+p(P_2)\to K+X)=\int_0^1 dx_1\int_0^1 dx_2\sum_f f_f(x_1)f_{\bar f}(x_2)\cdot\hat\sigma(q_f(x_1P)+\bar q_f(x_2P)\to K). \tag{3.1}$$

The simplest example of this kind is the Drell-Yan process, in which a massive lepton pair emerges from a $q\bar{q}$ annihilation in a proton-proton collision.

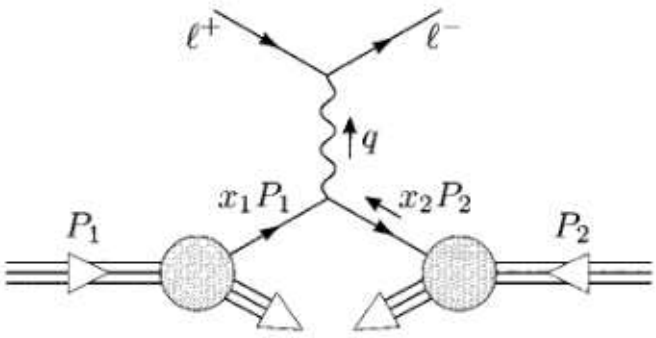

Figure 3.1: The Drell-Yan process.

We define

$$M^2 = q^2 \tag{3.2}$$

as the square of the invariant mass of the leptons. It is possible to parametrize the longitudinal momentum of the virtual boson with its rapidity Y, defined as

$$q^0 = M \cosh Y. \tag{3.3}$$

where q^0 is the time component of the four-momentum of the virtual boson in the pp center of mass frame. At leading perturbative order, it is possible to express the longitudinal fractions of the quark momenta in terms of M^2 and Y:

$$x_1 = \frac{M}{\sqrt{s}} e^Y, \qquad x_2 = \frac{M}{\sqrt{s}} e^{-Y}. \tag{3.4}$$

where $\sqrt{s}$ is the total energy in the center of mass frame of the colliding protons.

3.2 The electroweak partonic process

The Drell-Yan process $pp \to l^+l^- + X$ can be described, at the lowest order in the EW interaction, by the Feynman diagrams for Z^0 exchange and photon exchange, described in Figure 3.2. The corresponding Feynman amplitude can be written as

$$\mathcal{M} = \mathcal{M}_\gamma + \mathcal{M}_Z, \tag{3.5}$$

and the cross-section can be computed as

$$d\sigma \propto \sum |\mathcal{M}_\gamma + \mathcal{M}_Z|^2(\hat{s}, \hat{t}, \hat{u}), \tag{3.6}$$

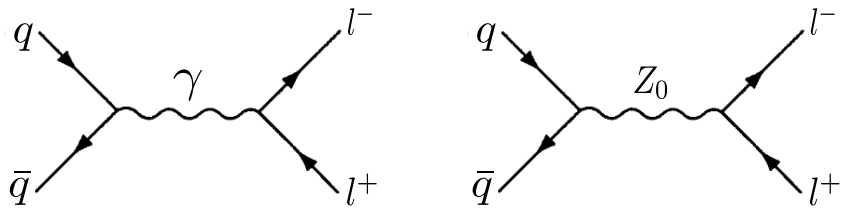

Figure 3.2: Leading contributions to the Drell-Yan process.

where the sum is taken over the spin and color degrees of freedom of the initial and final state fermions and $\hat{s},\ \hat{t},\ \hat{u}$ are the kinematical variables of the parton system.

However, while the coupling of a fermion to a photon has only a vector component, the coupling of the same fermion to the Z_0 is characterized by both vector and axial-vector components. Consequently, the cross-section exhibits parity-violating effects. Once a suitable reference frame is chosen, the differential cross-section at the leading order can be written as [5]

$$\frac{d\sigma}{d\cos\theta} = A(\hat{s})(1+\cos^2\theta) + B(\hat{s})\cos\theta, \tag{3.7}$$

where $\hat{s}$ is the total energy in the center of mass frame of the colliding partons. The term which depends linearly from $\cos\theta$ is asymmetric under parity transformation. Hence because of the vector and axial-vector couplings, the angular distribution for $q\bar{q} \to Z^0X \to l^+l^-X$ is asymmetric in $\cos\theta$. In order to minimize the effects of the unknown transverse momentum of the incoming quarks [13] a preferential reference frame is chosen. The angle θ^* is defined [12] as the polar angle of the negatively charged lepton relative to the incoming quark momenta in the rest of frame of the lepton pair (Collins-Soper reference frame) :

$$\cos\theta^* = f\frac{2}{M(l^+l^-)\sqrt{M^2(l^+l^-)+p_t^2(l^+l^-)}}[p^+(l^-)p^-(l+) - p^-(l^-)p^+(l^+)], \tag{3.8}$$

where

$$p^{\pm} = \frac{1}{\sqrt{2}}(E \pm p_z), \qquad\qquad f = \frac{|p_z(l^+l^-)|}{p_z(l^+l^-)}, \tag{3.9}$$

with E and p_z respectively the energy and the longitudinal momentum of the lepton pair. The Forward-Backward Asymmetry (A_{FB}) is defined as [14]:

$$A_{FB}(M_{l^+l^-}) = \frac{F(M_{l^+l^-}) - B(M_{l^+l^-})}{F(M_{l^+l^-}) + B(M_{l^+l^-})}, \tag{3.10}$$

where

$$F(M_{l^+l^-}) = \int_0^1 \frac{d\sigma}{d\cos\theta^*}d\cos\theta^*, \qquad B(M_{l^+l^-}) = \int_{-1}^0 \frac{d\sigma}{d\cos\theta^*}d\cos\theta^*. \tag{3.11}$$

The Forward-Backward Asymmetry is defined relative to the quark direction. At LHC, however, the initial state is symmetric. For this reason, it is necessary to define $\cos\theta^*$ with the extra sign factor f [15]; without that definition the asymmetry would vanish if measured

in symmetric intervals of rapidity, since the contributions to $F(M_{l^+l^-})$ and $B(M_{l^+l^-})$ would be equal but opposite in sign.

At LHC A_{FB} is therefore defined according to the sign of rapidity of the lepton pair [16]. For fixed rapidity, the longitudinal momenta of the quarks are determined by Eq. (3.4). Since valence quarks dominate at high values of x, it is more likely to find a quark with high x than a sea antiquark. Consequently, as the rapidity increases so does the probability that the quark direction and the boost direction coincide. Hence the value of A_{FB} depends on the kinematical region where the data are collected. If measurements are made in the forward region, where $x_1 \gg x_2$, the probability to find a sea antiquark with high momentum is lower then the probability to find a quark and thus the asymmetry is more easily observable.

The interest in the Forward-Backward Asymmetry lies in its relation with the electroweak mixing angle. In fact, a precise determination of A_{FB} enables a precise evaluation of $\sin^2\theta_W$.

Currently, $\sin^2\theta^l_{\text{eff}}$[1] is known very accurately from global fits to data (mostly from e^+e^- collisions), which are sensitive to electroweak parameters. The current best fit value is 0.23153 ± 0.00016 [19]. However, there is a certain tension between different inputs to global electroweak fits. In particular, the two most precise determinations (see Fig. 3.3) are about three sigma apart. A new experimental measurement of $\sin^2\theta_W$ is thus of great interest.

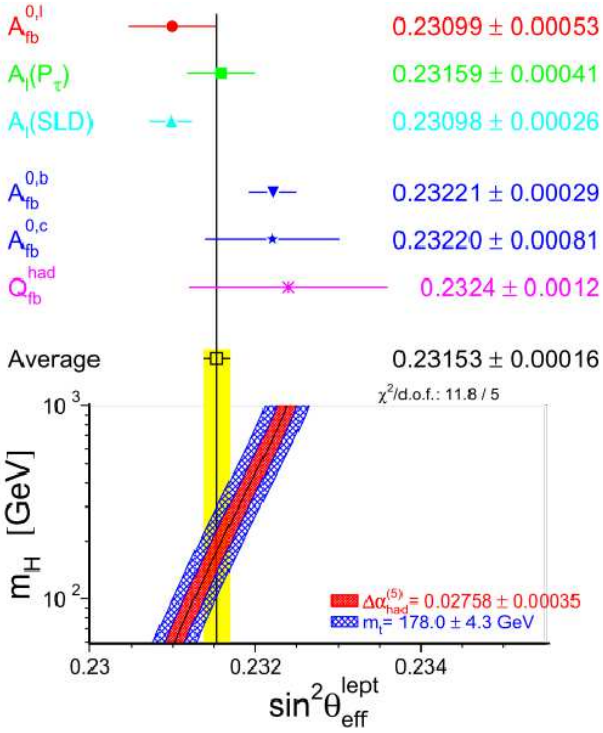

Figure 3.3: Comparison of $\sin^2\theta^l_{\text{eff}}$ derived from measurement depending on lepton couplings (top) and quark couplings (bottom). It is also shown the SM prediction for $\sin^2\theta^l_{\text{eff}}$ as a function of m_H.

[1] The relation between $\sin^2\theta^l_{\text{eff}}$ and $\sin^2\theta_{\text{W}}$ is well known. See for example [11].

3.3 Parton distributions

We have used different global set of parton distributions functions in order to inspect the impact of uncertainties on the Forward-Backward Asymmetry. The set of PDF used are NNPDF2.1, MSTW2008nlo and CT10. Those collaborations use different methods for evaluating the PDFs and their uncertainties. In this section we briefly summarize their different approaches.

In order to determinate PDFs at least seven independent functions are needed, which corresponds to the three light quarks and antiquarks and to the gluon distribution at some scale. If heavy quarks are taken into account, the number of functions increases. The problem which has to be solved thus implies the determination of a probability distribution in a function space. This is in principle an unsolvable task, because the experimental data are finite in number.

It is possible to get round this apparently unsolvable problem assuming a certain functional form for the parton distributions, justifying that assumption by the hypothesis of smoothness of the PDFs in x, with $0 \leq x \leq 1$. It is thus possible to represent PDFs with a finite accuracy on a finite basis of functions, and then with a finite number of parameters. There are different methods to optimize this parameterisation, given a certain accuracy and without introducing bias.

3.3.1 The "standard" approach: MSTW and CT10

In a standard approach PDFs are determined assuming for them a functional form with some limiting behaviours suggested by theory at small and large x and at a certain scale Q_0. Thus PDFs are thought to have the form

$$f_i(x, Q_0^2) = x^{\alpha_i}(1-x)^{\beta_i} g_i(x), \tag{3.12}$$

where the first two terms take into account the limiting behaviour and $g_i(x)$ tends to a constant at the limits. For example, the CT10 parameterisation [21] assumes the following functional form for valence quarks PDFs:

$$q_v(x, \mu_0) = q(x, \mu_0) - \bar{q}(x, \mu_0) = a_0 x^{\alpha_1}(1-x)^{\alpha_2} \exp(a_3 x + a_4 x^2 + a_5\sqrt{x}), \tag{3.13}$$

with parameters $a_1, \ldots a_5$ varied freely and $\mu_0 = 1.3$ GeV. The MSTW collaboration [22] uses a similar parameterisation for the up and down valence quarks:

$$xv(x, Q_0^2) = A_v x^{\delta_v}(1-x)^{\eta_v}(1 + \epsilon_v\sqrt{x} + \gamma_v x). \tag{3.14}$$

The total number of free parameters used may vary due to the different possible choices. CT10 parameterises the valence quark combinations $u_v = u - \bar{u}$, $d_v = d - \bar{d}$, the $\bar{u}$ and $\bar{d}$ distributions, the gluon, and $s = \bar{s}$ distribution (for simplicity an assumption of symmetry between the strangeness and anti-strangeness PDF is made), for a total number of 26 free parameters. MSTW on the other hand parameterises u_v, d_v, $s + \bar{s}$, $s - \bar{s}$, the gluon and also $\bar{u} \pm \bar{d}$ for a total of 28 free parameters.

Once a parameterisation has been chosen, the best fit values and the range of uncertainties of the parameters can be determined minimizing

$$\chi^2(\vec{a}) = \frac{1}{N_{\text{dat}}} \sum_{i,j} \left(d_i - \bar{d}_i(\vec{a})\right) \text{cov}_{ij} \left(d_j - \bar{d}_j(\vec{a})\right). \tag{3.15}$$

The sum runs over the data points, cov_{ij} is the experimental covariance matrix constructed with the experimental data d_i and $d_i(\vec{a})$ are the theoretical predictions obtained from calculations on the starting PDFs. The vector $\vec{a}$ represents the set of parameters chosen for the PDFs parameterisation at the initial scale Q_0.

Once the χ^2 has been defined, the best set of parameters is the one which provides the absolute minimum of χ^2 in the parameter space. Moreover, the variance of a observable $X(\vec{a})$, if linear error propagation is assumed, is

$$\sigma_X^2 = \sigma_{ij}\partial_i X \partial_j X, \tag{3.16}$$

where σ_{ij} is the covariance matrix of the parameters, which next to the minimum is given by

$$\sigma_{ij} = \partial_i \partial_j \bar{\chi}^2|_{\min}, \tag{3.17}$$

which is the Hessian matrix at the minimum of the unnormalized $\bar{\chi}^2 = N_{\mathrm{dat}}\chi^2$.

In principle, in the Hessian approach the 68% C.L. interval for the parameters can be evaluated as the ellipsoid in the parameter space which is the solution of the equation $\bar{\chi}^2 = \bar{\chi}^2_{\min} + 1$.

In such case (3.16) reduces to

$$\sigma_X^2 = \frac{1}{4}\sum_{k=1}^{N}[X(S_k^+) - X(S_k^-)]^2, \tag{3.18}$$

where $S_k^{\pm}$ are pairs of eigenvectors PDF sets which spans the hypersphere in the parameter space of radius 1, with parameters given by

$$a_i(S_k^{\pm}) = a_i^0 \pm e_{ik}. \tag{3.19}$$

Alternatively, asymmetric errors can be calculated as

$$(\sigma X)_+^2 = \sum_{k=1}^{N}\{\max[X(S_k^+) - X(S_0), X(S_k^-) - X(S_0), 0]\}^2, \tag{3.20}$$

$$(\sigma X)_+^2 = \sum_{k=1}^{N}\{\max[X(S_0) - X(S_k^+), X(S_0) - X(S_k^-), 0]\}^2, \tag{3.21}$$

where S_0 is the central set. In practice, it turns out that uncertainties determined in this way are unrealistically small. It is thus necessary to inflate all uncertainties by a suitable rescaling factor (tolerance). This suggests some fundamental underlying difficulty.

3.3.2 The Monte Carlo approach: NNPDF

The NNPDF collaboration bases the determination of parton distribution functions on a Monte Carlo approach, in conjuction with the use of neural networks as unbiased interpolants [23].

The difference between a Monte Carlo approach and a Hessian approach consists in the way the uncertainty are propagated from the parameter space to observables. We briefly summarize how uncertainties are computed in a Monte Carlo approach, and then we will examine how the approach has been used combined with neural networks as parton parameterisation by the NNPDF collaboration.

Whereas in a Hessian approach uncertainties are determined using linear error propagation from the covariance matrix σ_{ij}, assuming that parameters are Gaussianly distributed in the parameter space, the probability distribution in a Monte Carlo approach is provided by a sample of replicas of the whole parameter set. The central value of an observable X is then computed as the average of the observables X^i computed $N_{\rm rep}$ times using $N_{\rm rep}$ different parameter replica:

$$X = \frac{1}{N_{\rm rep}} \sum_i^{N_{\rm rep}} X^i. \tag{3.22}$$

The uncertainty is computed as the variance:

$$\sigma_X^2 = \frac{1}{N_{\rm rep}-1} \sum_i^{N_{\rm rep}} [X^i - X]^2. \tag{3.23}$$

In the Monte Carlo approach then the whole probability distribution can be determined from the sample of $N_{\rm rep}$ values of X computed.

In order to obtain correct estimations of the observables values and their uncertainties, it is necessary to start from a consistent distribution of parameter values. The procedure used can be summarized into two main stages:

1. Data replicas $F_i(1), \dots F_i(N)$ are generated from experimental data F_i. The ensamble of replicas is generated with the probability distribution of experimental data and it is large enough to reproduce their statistical properties. In practice, starting from data d_i with covariance matrix cov_{ij}, $N_{\rm rep}$ data replicas are generated, in such way that the mean value of the replicas of the nth data point tends to d_n, and the covariance matrix of the data replicas tends in the limit $N_{\rm rep} \to \infty$ to the original matrix.

2. In the second step one fits a set of parton distribution to each data replica. A best-fit parameter vector $\vec{a}^i$, $i = 1, \dots N_{\rm rep}$ is determined for each replica minimizing χ^2 Eq. (3.15), but the fit is performed on the data replica rather than on the original data. The PDFs can be parameterised in any preferred way, and then evolved to the scale of the data in order to minimize χ^2.

The problem of sampling the replica distribution in parameter space is then reduced to the construction of an adequate Monte Carlo representation of the experimental data. It is possible to check if an ensemble of replicas represents an accurate enough representation of data comparing means, variance and covariance and comparing the results obtained to the original data set.

As we have seen, in the standard approach a particular functional form, with a fixed number of parameters, is chosen, and the problems is reduced to performing a fit on the data in order to determine the value of those parameters. An obvious limitation of this method is that the choice of a particular functional form may be a source of bias. This problem is particularly delicate, as functional forms parameterised by a small number of parameters may be necessary in order for the fit to converge. Within a Monte Carlo approach, it is possible to choose a parameterisation with a large number of parameters, because one no longer expands about the absolute minimum of the χ^2. Neural networks are then a particularly convenient choice of parameterisation.

The NNPDF collaboration parameterises PDFs with neural networks arranged in layers where each layer communicates only with its next neighbour. A 2-5-3-1 neural networks is used with 37 free parameters for each PDF. As the six light flavours and antiflavours and the gluon are parameterised in this way, the total number of parameter is 259, to be compared to the typical number of parameters (about 30) of the CTEQ and MSTW parameterisations.

Chapter 4

Results

4.1 Introduction

Since the Forward-Backward Asymmetry is sensitive to $\sin^2\theta_W$, a precise measurement of A_{FB} may allow an accurate determination of the weak mixing angle. This measurement can be used together with other electroweak parameters to constrain the Higgs mass, and to perform precision test of the Standard Model [24, 25].

PDFs are expected to be one of the main source of uncertainty on A_{FB} . It is thus necessary to estimate their impact on the measurement of $\sin^2\theta_W$. In a future precise measurement of $\sin^2\theta_W$ it will be also necessary to determinate precisely the statistical uncertainty, and to compare it to the PDF uncertainties for fixed integrated luminosity.

We have studied A_{FB} as a function of the invariant mass of the lepton pair, limiting our study at the Born level. We have first studied the sensitivity of A_{FB} to small variations of $\sin^2\theta_W$. We have then studied PDF and statistical uncertainties on A_{FB} and we have compared those uncertainties to the sensitivity, in order to obtain a first qualitative estimate of the impact of the uncertainties on the measurement of the Weinberg angle. We have then studied at a quantitative level the impact of the PDF uncertainties by means of a template fitting method. After studying the PDF uncertainties, we have focused on the statistical uncertainties, and we have combined the results in order to obtain a complete estimate of the impact of the main uncertainties on the measurement of $\sin^2\theta_W$ from A_{FB} at the LHC.

The chapter is organized as follows. In Sect. 4.2 we illustrate the cuts used and the event generator settings. In Sect. 4.3 we discuss the sensitivity of A_{FB} to the Weinberg angle. In Sect. 4.4 we show the results which we have obtained studying A_{FB} as a function of the invariant mass and we compare the uncertainties to the sensitivity of A_{FB} to $\sin^2\theta_W$. In Sect. 4.5 we give a more refined estimate of the impact of the PDF uncertainties on the value of $\sin^2\theta_W$. We show in Sect. 4.6 the results for the estimate of the statistical uncertainties on the measurement of $\sin^2\theta_W$. We sum up the results in Sect. 4.7 and in Sect. 5 we draw our conclusions.

4.2 Generation of events and settings

We have inspected the sensitivity of A_{FB} to the weak mixing angle by studying differential distributions in Neutral Current Drell-Yan production. We have studied the lepton pair's invariant mass distribution between 60 and 120 GeV with a bin size of 0.5 GeV.

We have generated Drell-Yan neutral current events at Born level with the event generator HORACE. Monte Carlo event generators are very useful tools because they allow a very flexible and realistic simulation of the detector set-up, and in particular of the detector acceptances.

We have generated events using the three global PDF sets NNPDF2.1, MSTW 2008 and CT10 with a statistics of 10^9 events. The events have been generated in two scenarios: ATLAS/CMS and LHCb. In both scenarios we have considered LHC collisions at 7 TeV, and we have imposed at 25 GeV the minimum transverse momentum p_t of each lepton. We have finally imposed two different acceptances for the rapidity of each lepton: in ATLAS/CMS kinematics both leptons are identified in $|\eta| < 2.5$, whereas in LHCb kinematics the leptons are identified in $2.0 < \eta < 4.5$.

The results have been obtained using the following values for the input parameters:

$$\begin{array}{lll} G_\mu = 1.16637\ 10^{-5}\ \text{GeV}^{-2} & m_W = 80.398\ \text{GeV} & m_Z = 91.1876\ \text{GeV} \\ \Gamma_W = 2.141\ \text{GeV} & \sin^2\theta_W = 1 - m_W^2/m_Z^2 & m_H = 115\ \text{GeV} \end{array}$$

EW corrections modify the tree level relation between the Weinberg angle and the masses of the weak bosons at the per cent level. However, despite the fact that these corrections modify considerably the effective value of $\sin^2\theta_W$ they have a negligible effect on the computation of the uncertainties since they depend very weakly on the central value.

4.3 A_{FB} sensitivity to the weak mixing angle

The study of the sensitivity of A_{FB} to the weak mixing angle allows one to compare PDF and statistical uncertainties to the sensitivity and to obtain an estimate of their impact. In this section we describe how we have estimated the sensitivity of A_{FB} to variations of the weak mixing angle and we show the results.

In order to inspect the sensitivity of A_{FB} to the weak mixing angle we have generated new invariant mass distributions in which we have changed the values of the input parameters. Since the Weinberg angle is not among the input parameters, we have obtained its variation by varying the mass of the W boson (recall Eq. (2.5)). This choice, that one would make in a realistic situation, is motivated by the fact that among the input parameters the W boson mass is the value which is known with the worst experimental accuracy.

We have considered the differences in the Forward-Backward Asymmetry obtained varying m_W by 5, 10 and 20 MeV. With such variations the value of $\sin^2\theta_W$ varies approximately by 0.0001, 0.0002, 0.0004. We estimate the sensitivity of A_{FB} to the Weinberg angle considering the discrepancy between the two distributions obtained varying the W mass of $\pm\delta$.

We show in Fig. 4.1 the absolute and relative sensitivity of A_{FB} to the Weinberg angle obtained by considering the distributions obtained in the ATLAS/CMS kinematics, while in Fig. 4.2 we show the results in the LHCb kinematics. In both the kinematical regions the sensitivity is greater in the central region of the plot.

In Fig. 4.3 we compare the sensitivities obtained in the ATLAS/CMS kinematics with those obtained in the LHCb kinematics. As we have already pointed out, since the Forward-Backward Asymmetry is favoured is the LHCb kinematics, in this kinematical region the sensitivity to the Weinberg angle is greater than in the ATLAS/CMS kinematics.

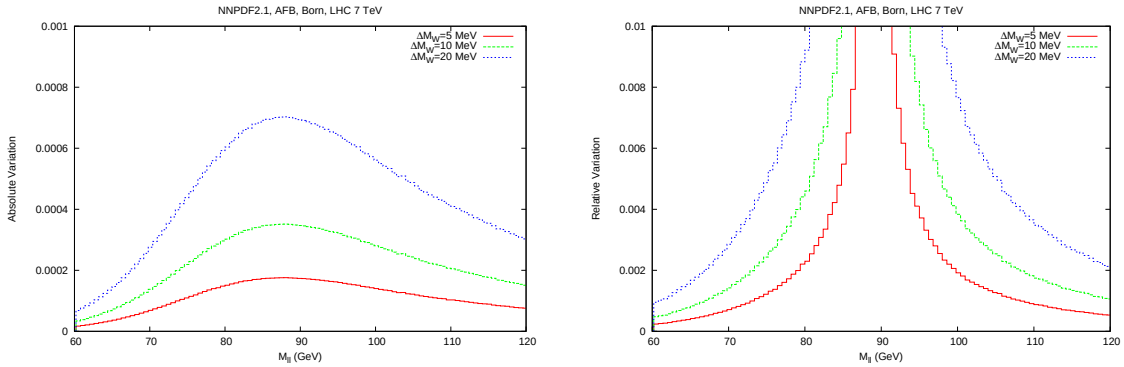

Figure 4.1: Absolute (left) and relative (right) sensitivity of A_{FB} to the Weinberg angle in the ATLAS/CMS kinematics, computed with PDFs of the NNPDF collaboration.

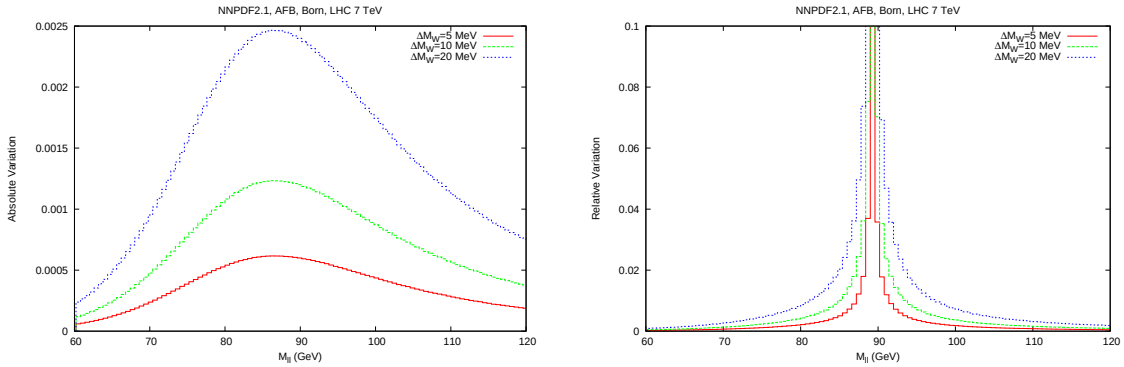

Figure 4.2: Absolute (left) and relative (right) sensitivity of A_{FB} to the Weinberg angle in the LHCb kinematics, computed with PDFs of the NNPDF collaboration.

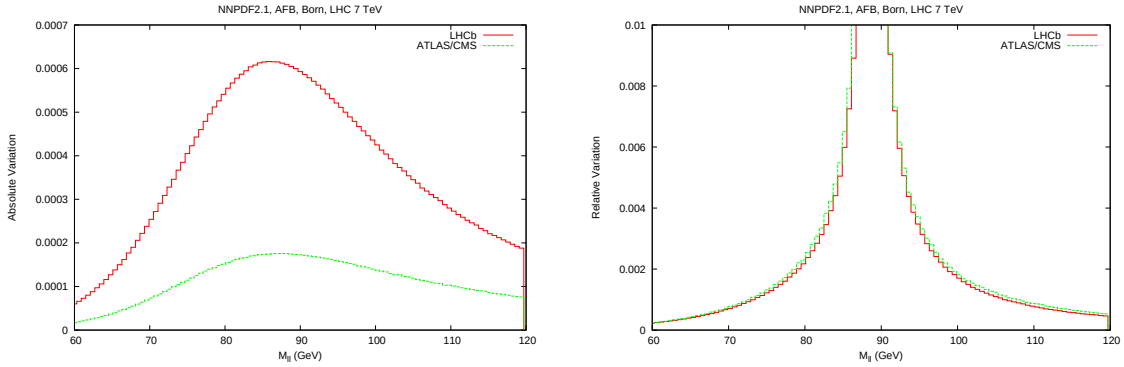

Figure 4.3: Comparison between the results obtained with PDFs from NNPDF collaboration with ATLAS/CMS and LHCb acceptances, with $\Delta m_W = 5$ MeV. On the left we show the absolute and on the right the relative sensitivity.

4.4 PDF and statistical uncertainties on A_{FB}

It is possible to obtain a first qualitative estimate of the impact of PDF and statistical uncertainties on the determination of $\sin^2\theta_W$ by the comparison of PDF and statistical uncertainties on A_{FB} to the sensitivity of A_{FB} to the weak mixing angle. In this section we present the results obtained studying the impact of PDF and statistical uncertainties on A_{FB} and we compare the uncertainties to the sensitivity of A_{FB} to variations of $\sin^2\theta_W$.

We study the invariant mass distribution in the two kinematical regions considered and we compare the results obtained with the different global PDF sets. We have followed the prescriptions provided by each collaboration in order to compute the PDF uncertainties. We recall that the NNPDF collaboration estimates the uncertainties as the standard deviation of the $N_{\rm rep}$ members

$$\sigma^2_{A_{FB}}(M_{l^+l^-}) = \frac{1}{N_{\rm rep}-1}\sum_i^{N_{rep}}[A^i_{FB}(M_{l^+l^-}) - A_{FB}(M_{l^+l^-})]^2, \tag{4.1}$$

while the CTEQ and the MSTW collaborations compute uncertainties in a Hessian approach:

$$\sigma_{A_{FB}}(M_{l^+l^-}) = \frac{1}{2}\sqrt{\sum_i^{N_{rep}/2}[A^{i(+)}_{FB} - A^{i(-)}_{FB}]^2}. \tag{4.2}$$

Furthermore, as the the CTEQ collaboration provides uncertainties in the 90% C.L. interval it is necessary to divide Eq. (4.2) by the rescaling factor $C_{90} = 1.64485\ldots$ to obtain the 68 % C.L. intervals, assuming gaussian scaling of the uncertainties. Finally, the uncertainties $\sigma^i_{A_{FB}}(M_{l^+l^-})$ on the single members have been calculated from the uncertainties on the forward and backward distributions as

$$\begin{aligned}\sigma^i_{A_{FB}}(M_{l^+l^-}) &= \sqrt{\left(\frac{\partial A^i_{FB}(M_{l^+l^-})}{\partial F^i(M_{l^+l^-})}\right)^2\sigma^2_{F^i(M_{l^+l^-})} + \left(\frac{\partial A^i_{FB}(M_{l^+l^-})}{\partial B^i(M_{l^+l^-})}\right)^2\sigma^2_{B^i(M_{l^+l^-})}} = \\ &= \sqrt{\frac{4(B^i(M_{l^+l^-}))^2}{(F^i(M_{l^+l^-})+B^i(M_{l^+l^-}))^4}\sigma^2_{F^i(M_{l^+l^-})} + \frac{4(F^i(M_{l^+l^-}))^2}{(F^i(M_{l^+l^-})+B^i(M_{l^+l^-}))^4}\sigma^2_{B^i(M_{l^+l^-})}}.\end{aligned} \tag{4.3}$$

We have calculated the statistical uncertainty with different integrated luminosities as

$$\begin{aligned}\sigma^i_{stat}(M_{l^+l^-}) &= \sqrt{\left(\frac{\partial A^i_{FB}}{\partial F^i}\right)^2\sigma^2_{stat\ F^i} + \left(\frac{\partial A^i_{FB}}{\partial B^i}\right)^2\sigma^2_{stat\ B^i}} = \\ &= \sqrt{\frac{4(B^i)^2}{(F^i+B^i)^4}\frac{(F^i)^2}{F^i\mathcal{L}} + \frac{4(F^i)^2}{(F^i+B^i)^4}\frac{(B^i)^2}{B^i\mathcal{L}}},\end{aligned} \tag{4.4}$$

since the statistical uncertainties on the forward and on the backward distributions are respectively

$$\sigma_{stat\ F^i} = \frac{F^i}{\sqrt{F^i\mathcal{L}}} \qquad\qquad \sigma_{stat\ B^i} = \frac{B^i}{\sqrt{B^i\mathcal{L}}}. \tag{4.5}$$

We first present the results we have obtained in the ATLAS/CMS kinematics. We finally consider the results obtained in the LHCb kinematics and we make a comparison between the two kinematical regions.

4.4.1 ATLAS/CMS kinematics

We show the results obtained for the ATLAS/CMS kinematics and we compare the predictions of the three global PDF sets considered. We found that the predictions for the Forward-Backward Asymmetry obtained with the different PDF sets are consistent, as Fig. 4.4 shows.

In Fig. 4.5 we show how the uncertainties depend on the invariant mass of the lepton pair. The results obtained with the three PDF sets in this case are quite different, since the uncertainties range between 2% (MSTW08) and 8% (NNPDF2.1).

In Fig. 4.6 we compare the results of the different PDF sets we have considered. On the left of Fig. 4.6 we show the ratios between the values of the Forward-Backward Asymmetry obtained with different PDF sets. We observe that the discrepancies between the results obtained with NNPDF2.1 and CT10 are at the 2% level, whereas the discrepancies between the results obtained with those sets and the results obtained with MSTW08 are at the 5% level. Obviously the discrepancies diverge at the Z peak, where the asymmetry tends to vanish. On the right of Fig. 4.6 we show the ratio between the PDF uncertainties calculated with the PDF sets considered. In particular, we observe that the uncertainties obtained with PDFs from the MSTW08 collaboration are rather smaller than the uncertainties computed with the other two global sets.

In Fig. 4.7 we show the statistical uncertainties obtained with PDFs from the NNPDF collaboration computed with different integrated luminosities. Since the statistics is greater at the Z pole, the statistical uncertainty is smaller in that zone.

We finally show in Fig. 4.8 a comparison between the different sources of uncertainties considered and the sensitivity to the Weinberg angle. We observe that the uncertainties are comparable to the sensitivity only in the central region of the plot, whereas in the outer regions PDF and statistical uncertainties are rather greater than the sensitivity. Moreover, we observe that an integrated luminosity of 100 fb^{-1} is needed in order to obtain a statistical uncertainty comparable to the sensitivity.

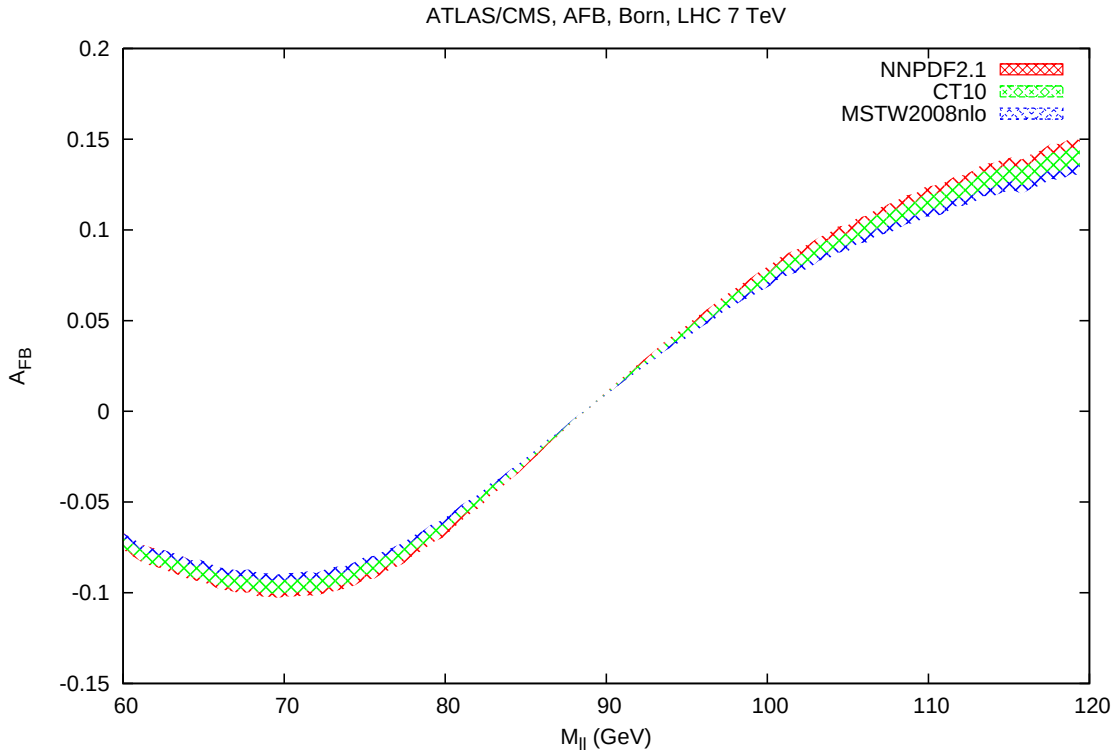

Figure 4.4: The Forward-Backward Asymmetry with uncertainty error bands calculated with the three global PDF sets considered.

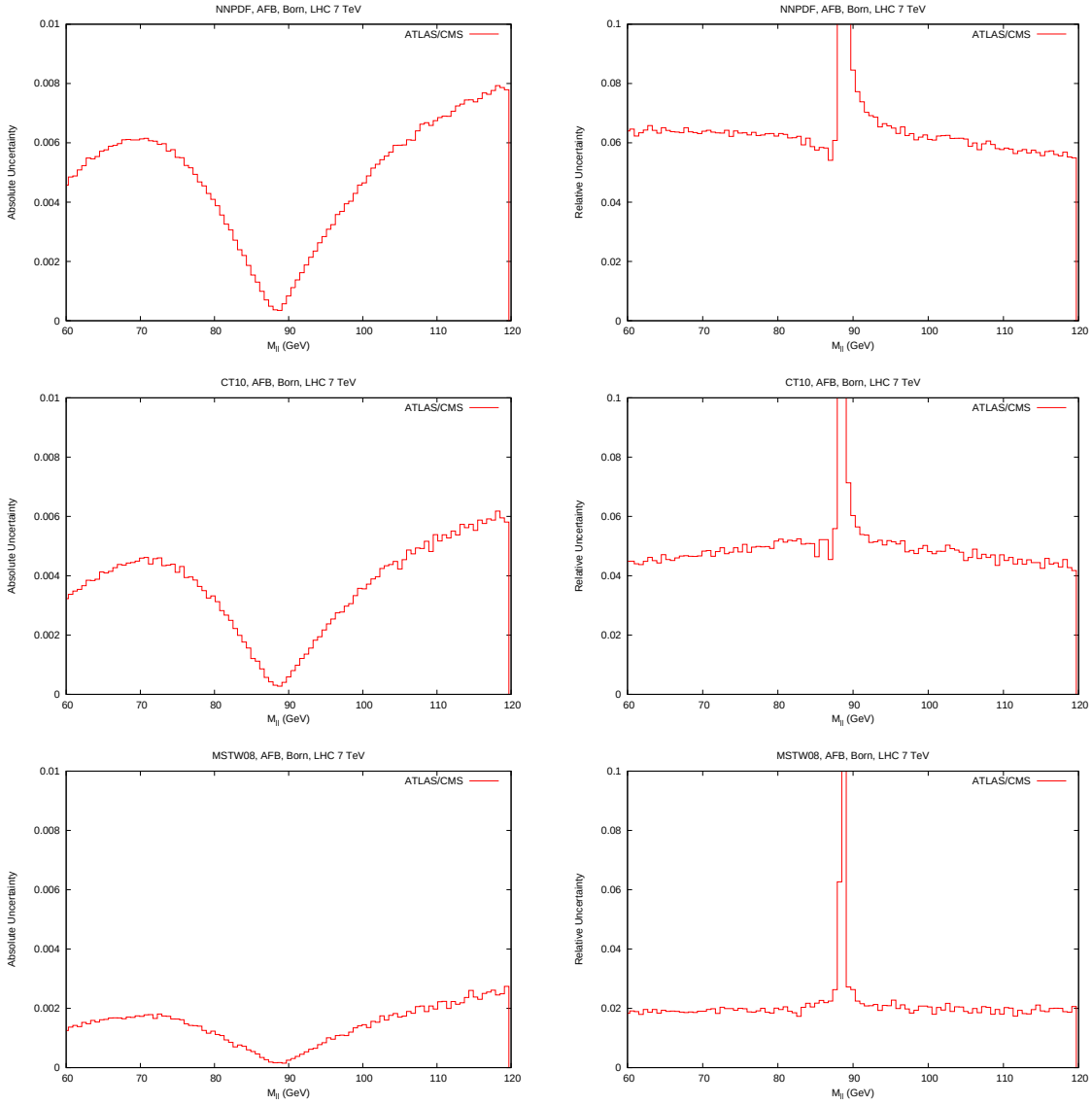

Figure 4.5: Absolute (left) and relative (right) PDF uncertainties for A_{FB} obtained with the different PDF sets. From top to bottom: NNPDF; CT10; MSTW.

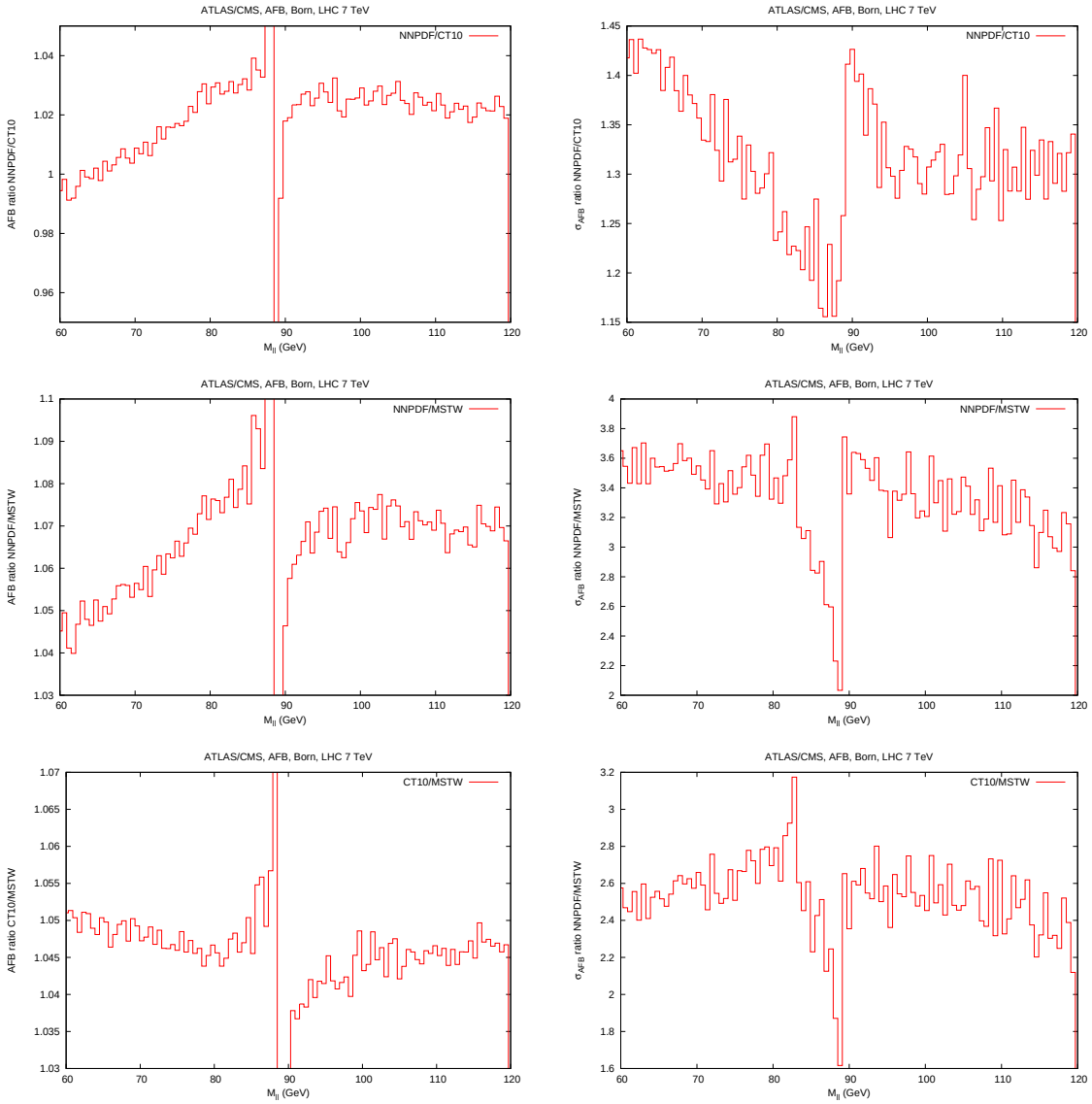

Figure 4.6: Comparison between the values of A_{FB} obtained with the different PDF sets and between their uncertainties. In the pictures whe show the ratio between A_{FB} (right) and the ratio between A_{FB} uncertainties obtained with different PDF sets (left). From top to bottom: comparison between CT10 and NNPDF results; comparison between NNPDF and MSTW results; comparison between MSTW and CT10 results.

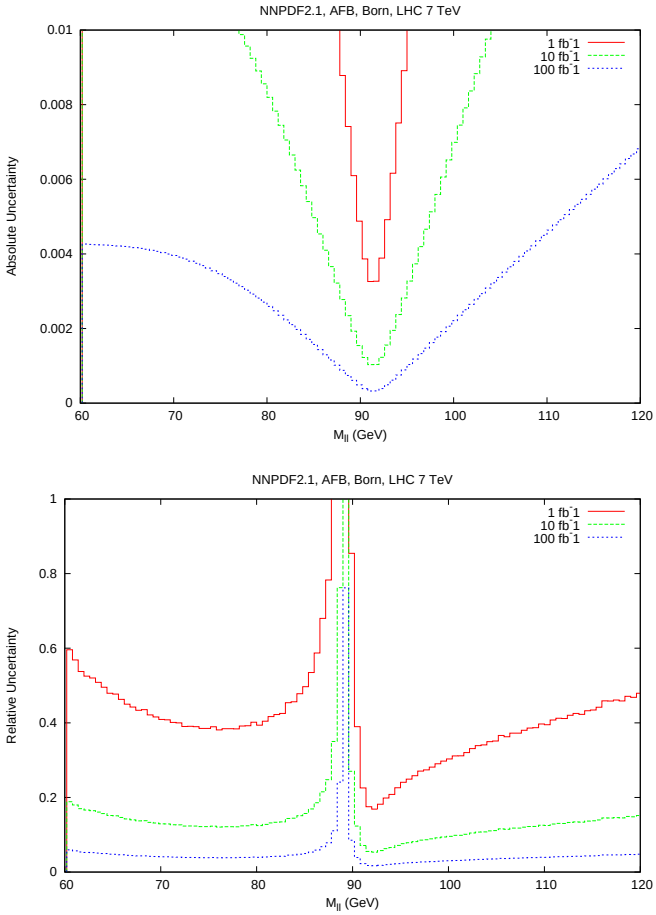

Figure 4.7: Absolute (left) and relative (right) statistical uncertainties on A_{FB} with different integrated luminosities in the ATLAS/CMS kinematics, computed with PDFs of the NNPDF collaboration.

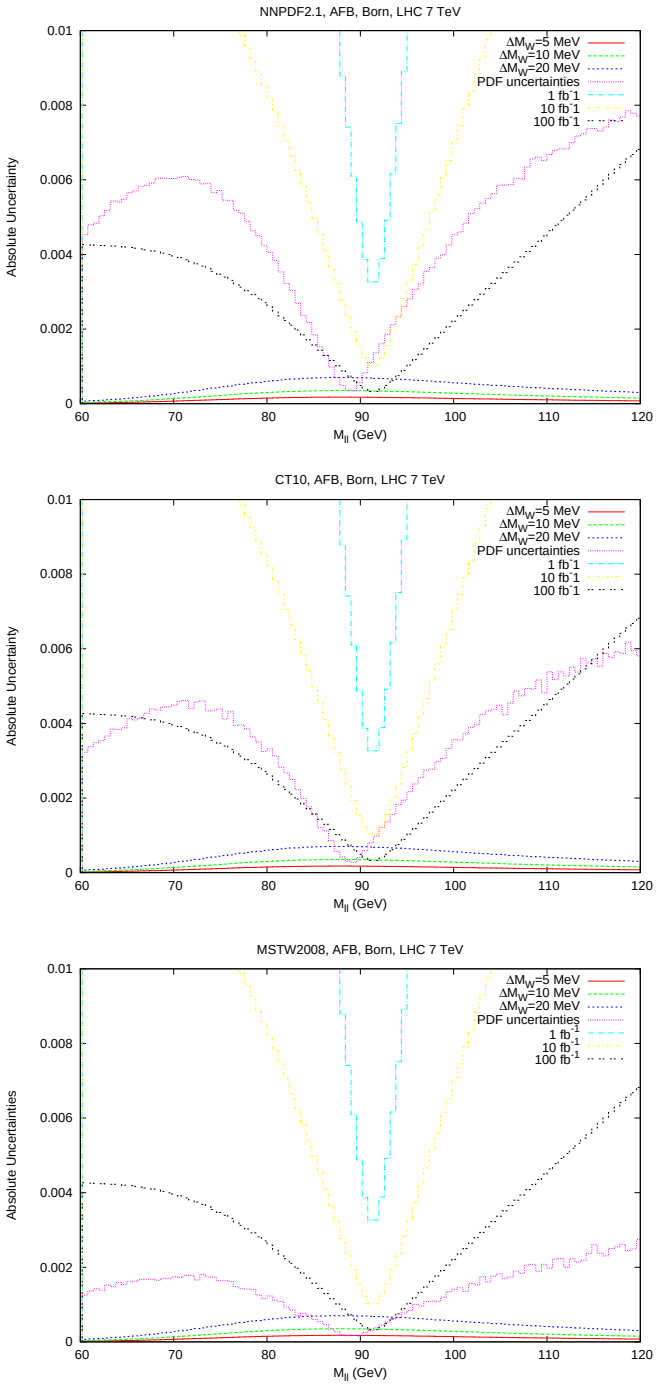

Figure 4.8: Comparison of the PDF uncertainties with the statistical uncertainties and with the sensitivity to the electroweak mixing angle at ATLAS/CMS. From top to bottom: NNPDF results; CT10 results; MSTW results. The statistical uncertainties and the sensitivity to the weak mixing angle are obtained with PDFs provided by the NNPDF collaboration.

4.4.2 LHCb kinematics

We show the results obtained for the LHCb kinematics with different PDF sets. The results obtained with such settings are compared to the results obtained with the cuts used in the ATLAS/CMS kinematics. We found that the predictions for the Forward-Backward Asymmetry computed with the PDF sets considered are similar also in the new kinematical region, as Fig. 4.9 shows. In Fig. 4.10 it is possible to appreciate how the Forward-Backward Asymmetry is particularly favoured in the LHCb kinematics.

We show in Fig. 4.11 the absolute and relative uncertainties obtained with the different PDF sets in function of the invariant mass. We observe that the uncertainties are at the 1.5% level for all the PDF sets considered.

In Fig. 4.12 we compare the results obtained with the different PDF sets considered. On the left of Fig. 4.12 we show a comparison between the values of A_{FB} that we have obtained with the three PDF sets considered. The discrepancies between the values obtained with CT10 and NNPDF are below the 1% level, whereas the discrepancies between CT10 and MSTW and between NNPDF and MSTW are at the 2% level, but they decrease at the 1% level for $M_{ll} > 100$ GeV. On the right of Fig. 4.12 the uncertainties obtained with the three PDF sets considered are compared. We observe that also in the LHCb kinematical settings the MSTW uncertainties are lightly smaller.

In Fig. 4.13 we show the absolute and relative statistical uncertainty with an integrated luminosity of 1, 10, 100 fb^{-1}. The statistical uncertainty is smaller at the Z pole since in that zone the statistics is greater.

In Fig. 4.14 we compare PDF and statistical uncertainties obtained in the ATLAS/CMS kinematics with those obtained in the LHCb kinematics. The absolute PDF uncertainties in the two kinematical regions are comparable, while the relative PDF uncertainties in the LHCb settings are consequently reduced by approximately the same factor which relates the asymmetry in the two regions.

Finally, Fig. 4.15 shows a comparison between the different sources of uncertainties considered and the sensitivity to the Weinberg angle. We observe that in this kinematical settings the region of the plot where the PDF uncertainties and the sensitivity are comparable is greater than the one in the ATLAS/CMS settings. We finally observe that an integrated luminosity of 100 fb^{-1} is needed in order to obtain a statistical uncertainty comparable to the sensitivity and to the PDF uncertainties.

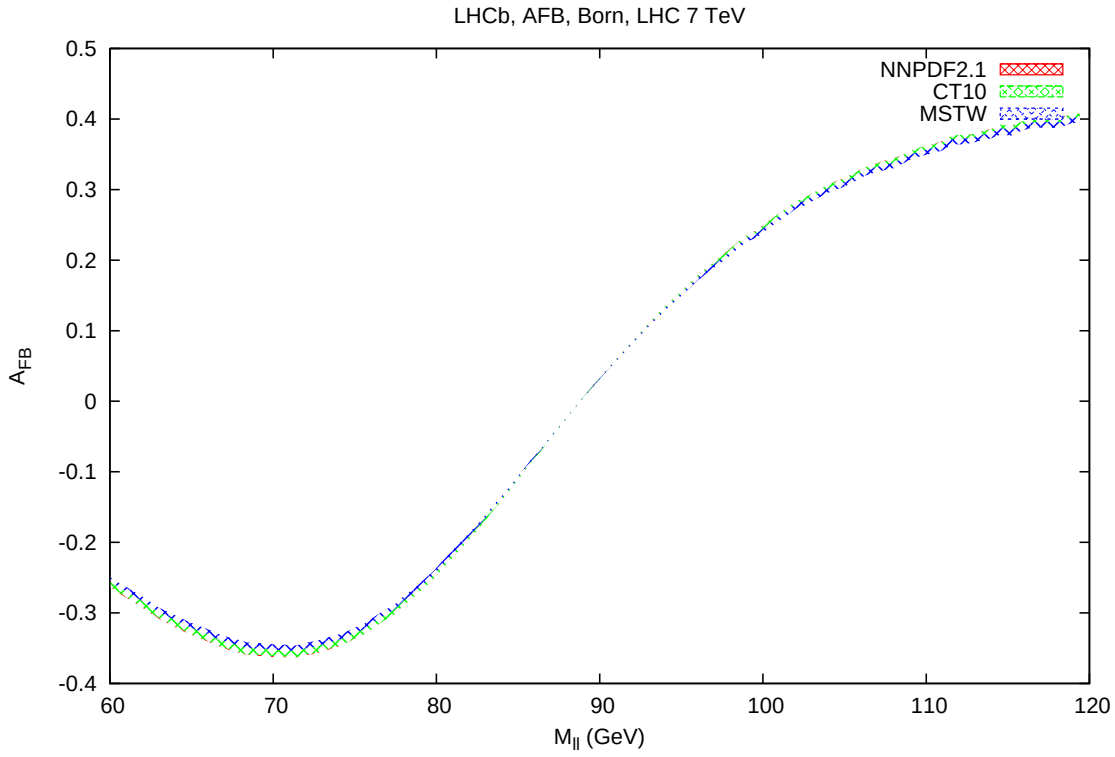

Figure 4.9: The Forward-Backward Asymmetry with uncertainty error bands calculated with the three global PDF sets considered.

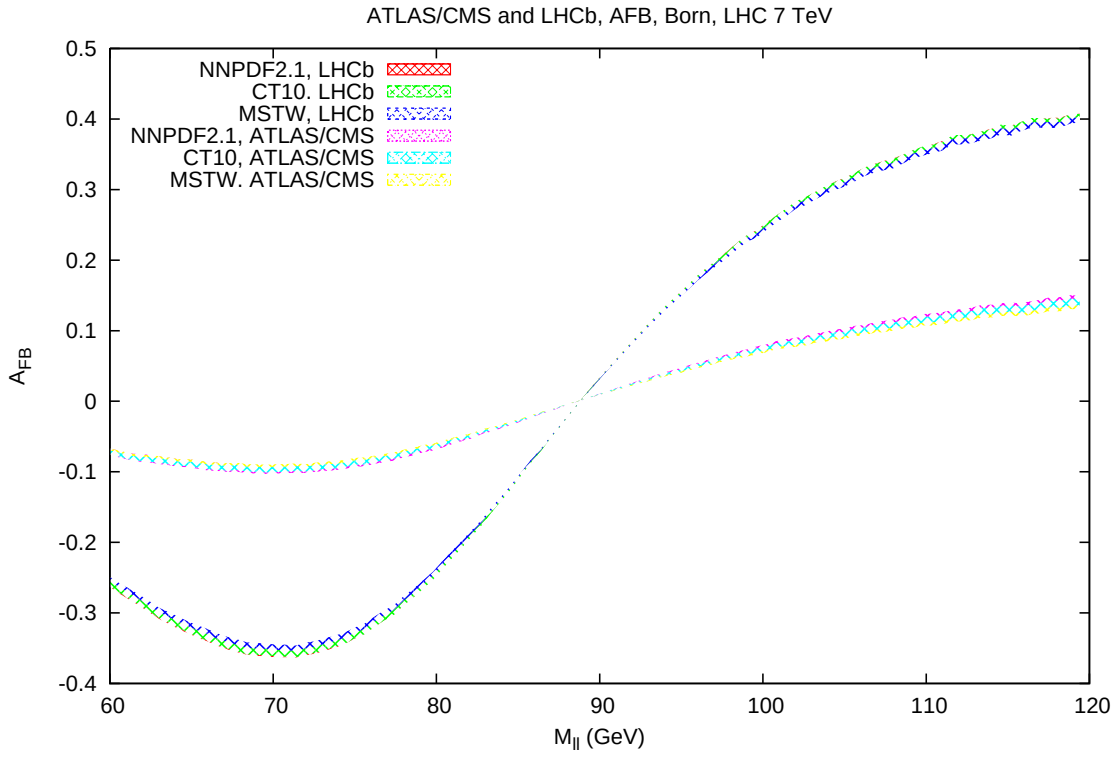

Figure 4.10: Comparison between the Forward-Backward Asymmetry with uncertainty error bands calculated with the three global PDF sets considered in both kinematical regions.

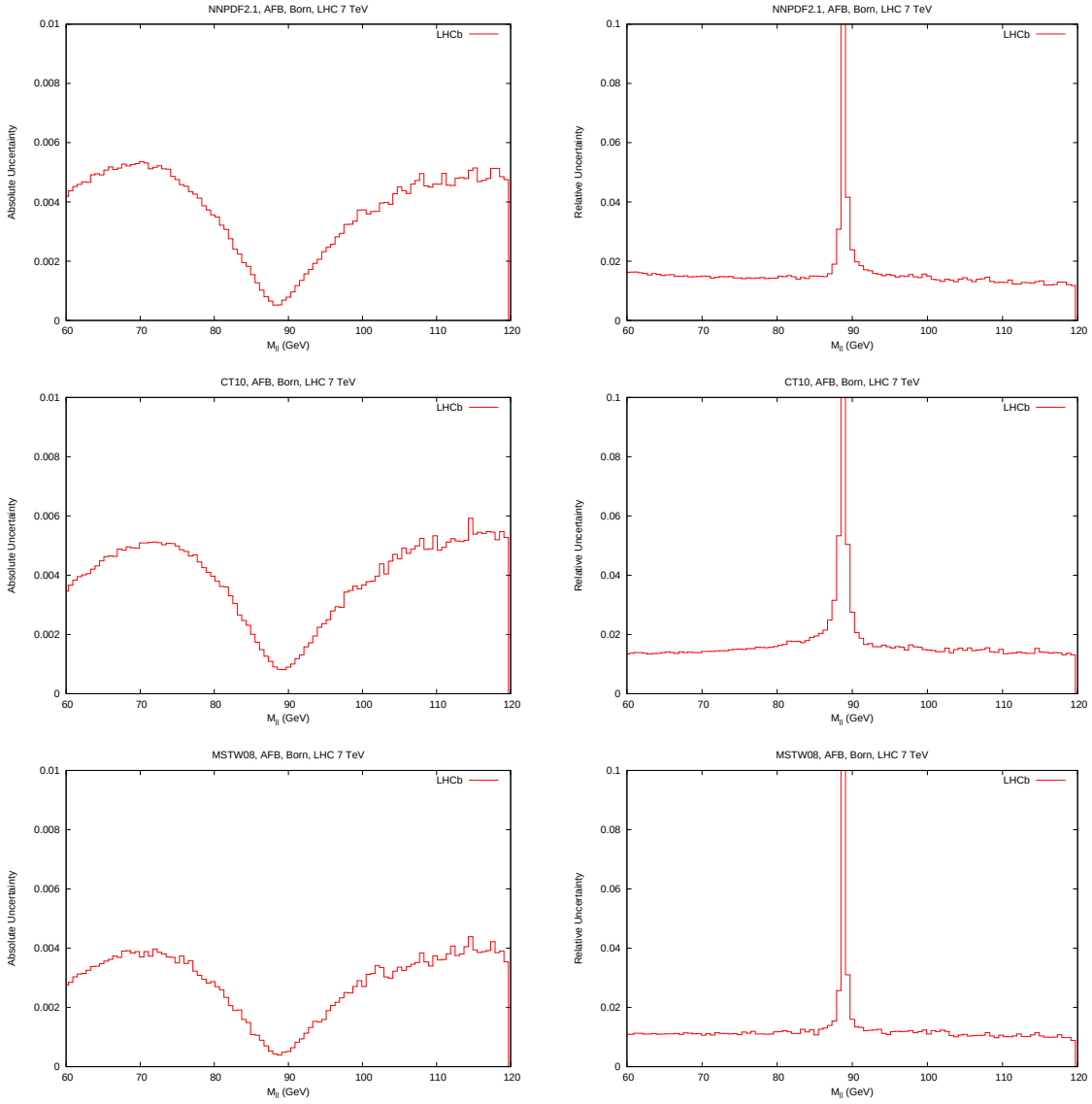

Figure 4.11: Absolute (left) and relative (right) PDF uncertainties for A_{FB} obtained with the different PDF sets. From top to bottom: NNPDF; CT10; MSTW.

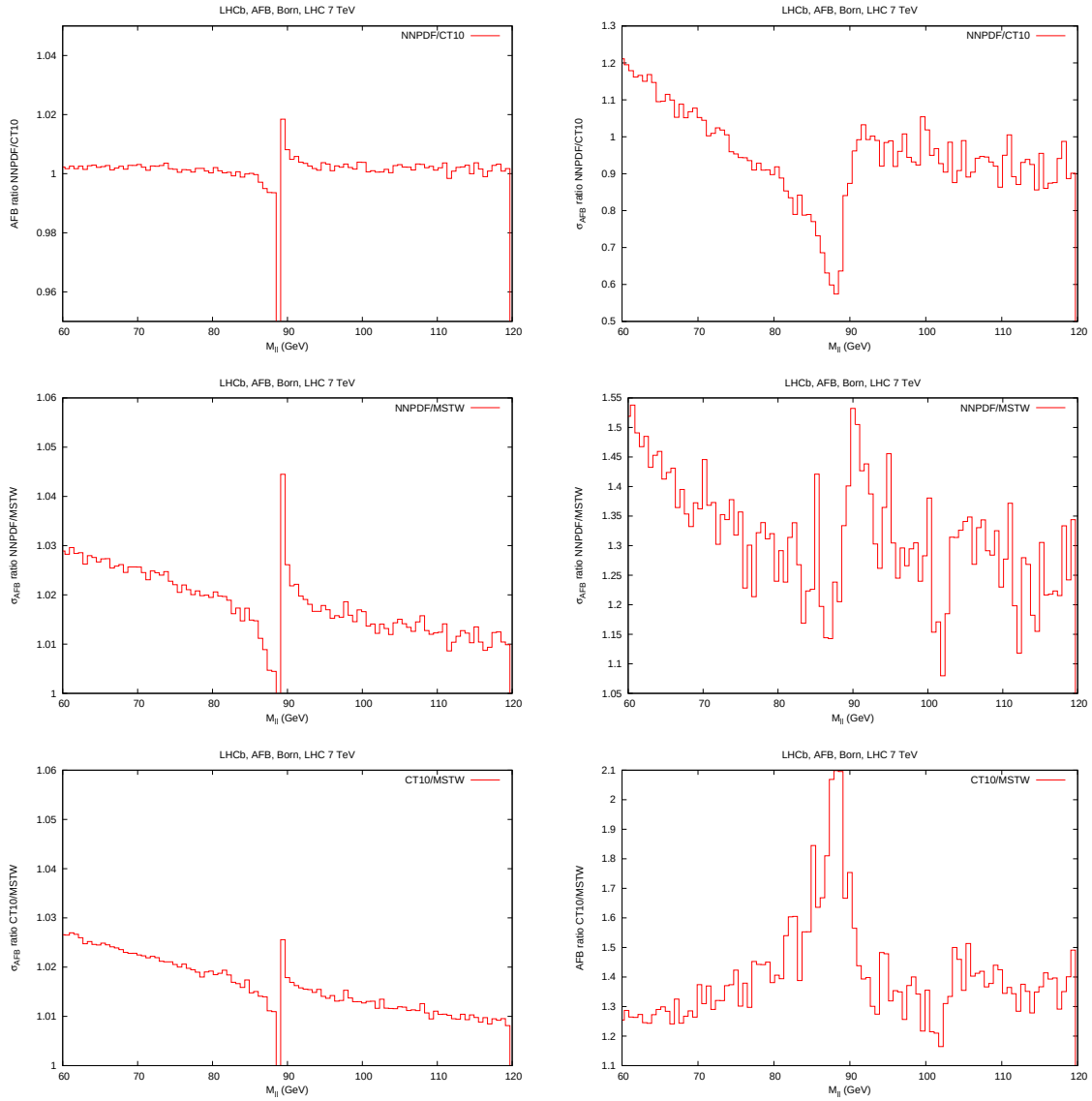

Figure 4.12: Comparison between the values of A_{FB} obtained with the different PDF sets and between their uncertainties. In the pictures we show the ratio between A_{FB} (right) and the ratio between A_{FB} uncertainties (left) obtained with different PDF sets. From top to bottom: comparison between CT10 and NNPDF results; comparison between NNPDF and MSTW results; comparison between MSTW and CT10 results.

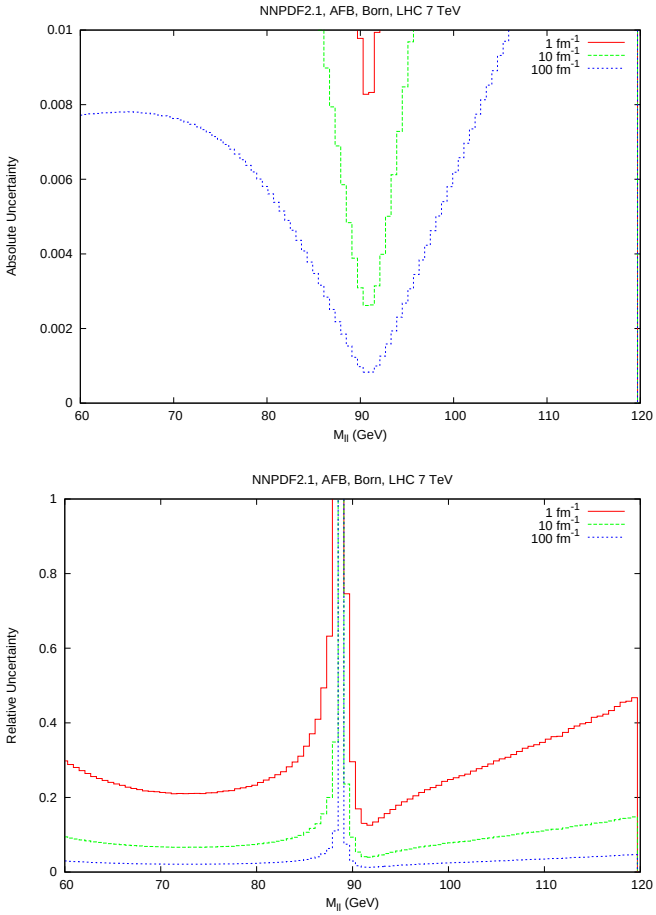

Figure 4.13: Absolute (left) and relative (right) statistical uncertainties for A_{FB} with different integrated luminosities in the LHCb kinematics, computed with PDFs of the NNPDF collaboration.

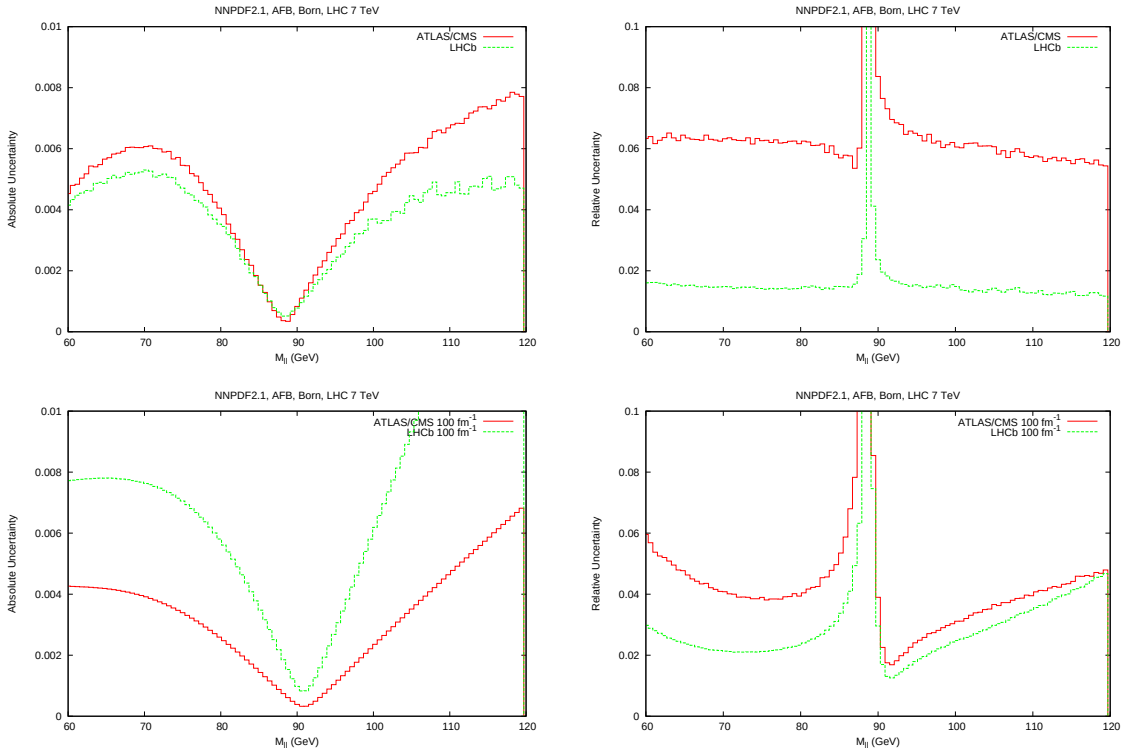

Figure 4.14: Comparison between the results obtained with PDFs from NNPDF collaboration with ATLAS/CMS and LHCb acceptances. From top to bottom: absolute (left) and relative (right) uncertainties for A_{FB}; absolute (left) and relative (right) statistical uncertainties with $\mathcal{L} = 100$ fb^{-1}.

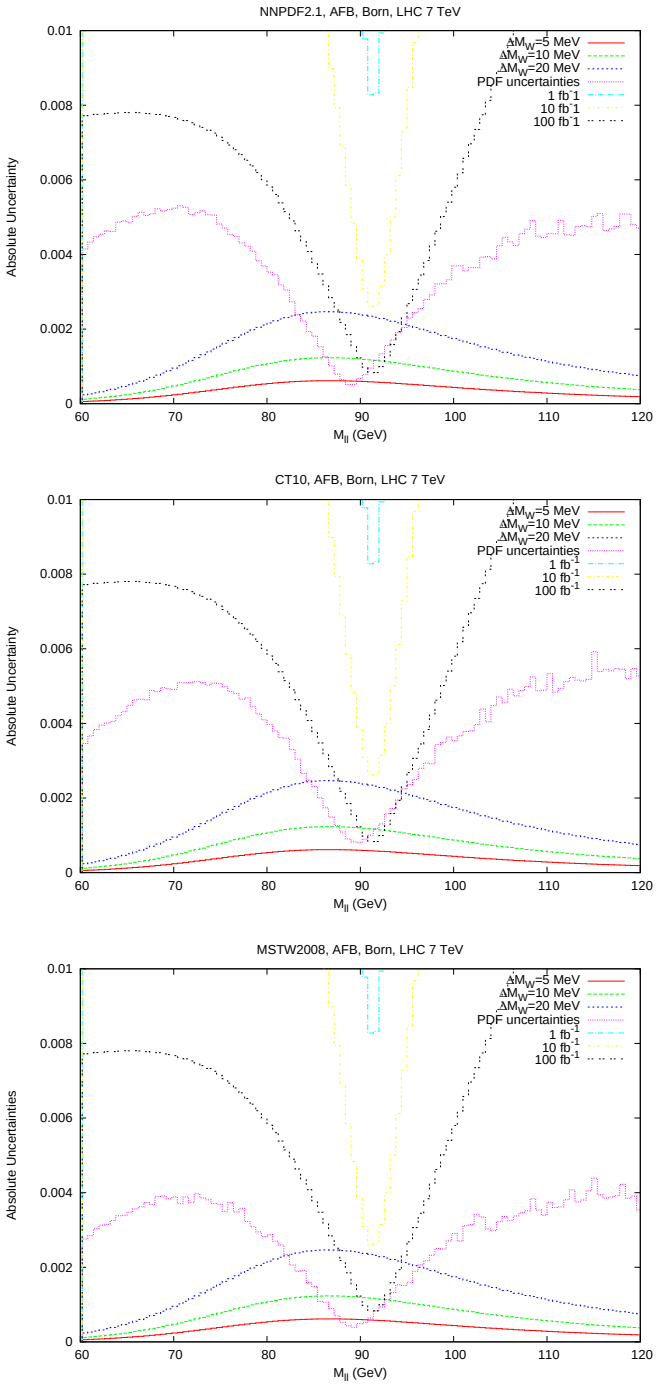

Figure 4.15: Comparison of the PDF uncertainties with the statistical uncertainties and with the sensitivity to the electroweak mixing angle at LHCb. From top to bottom: NNPDF results; CT10 results; MSTW results. The statistical uncertainties and the sensitivity to the weak mixing angle are obtained with PDFs provided by the NNPDF collaboration.

4.5 PDF uncertainties by template fitting method

We observe from Figs. 4.8 and 4.15 that the sensitivity of A_{FB} to the weak mixing angle and the PDF uncertainties are comparable only between 80 and 100 GeV, whereas in the outer regions of the plot the PDF uncertainties are considerably greater than the sensitivity. In order to precisely quantify the impact of the PDF uncertainties on a future measurement of $\sin^2\theta_W$ it is necessary a more refined method. In this section we describe the method we used and we show the results we obtained.

4.5.1 General strategy

We used a template fitting method in order to explore more precisely the sensitivity of A_{FB} to the value of $\sin^2\theta_W$. This approach has been applied in Ref. [26] to the evaluation of the PDF uncertainties in the determination of the W mass at the Tevatron and the LHC.

The method consists in the generation of several template distributions computed by varying the input parameters, in order to obtain theoretical models which differ one to the other by the fact that all the input parameters are fixed but the value of $\sin^2\theta_W$. The templates are then compared with each member of a particular PDF set. We associate to each member a preferred value of $\sin^2\theta_W$ which depends on the template which better fits to the results obtained with that member. It is then possible to estimate the impact of the PDF uncertainties studying the spread in $\sin^2\theta_W$ induced by the members of the PDF sets considered.

We have generated the templates using the central set of NNPDF2.1 parton distributions, and varying m_W around the nominal mass $m_W^0 = 80.398$ GeV with a range of $\pm$ 0.100 GeV and a separation interval of 0.005 GeV. We have then generated new distributions with $m_W = m_W^0$ for each member of the PDF sets considered using the same event generator of the templates. Each template has been compared with the $N_{\rm rep}$ members of each PDF set and for each member $k = 1, \dots N_{\rm rep}$ it has been constructed a reduced χ^2 function, defined as

$$\chi^2_{j,k} = \frac{1}{N_{\rm bins}} \sum_i^{N_{\rm bins}} \frac{\left(A^k_{FB_i} - A^j_{FB_i}\right)^2}{(\sigma^k_i)^2 + (\sigma^j_i)^2} \qquad\qquad j = 1, \dots N_{\rm temp}. \tag{4.6}$$

For each member there exists a value m_W^k (and equivalently $\sin^2\theta_W^k$) which minimizes $\chi^2_{j,k}$. Each member induces a shift $\Delta m_W^k = m_W^k - m_W^0$ between the preferred value m_W^k and the nominal mass. It is finally possible to estimate the impact of PDF uncertainties on the measurement of $\sin^2\theta_W$ computing the spread of the preferred values following the prescriptions of each collaboration.

4.5.2 Numerical Results

In this section we present the results we have obtained with the template fitting method described above in both kinematical regions considered in this study.

Table 4.1 shows the results obtained when performing the fitting procedure on the Born level invariant mass distribution in the ATLAS/CMS kinematics. We denote with $\delta_{\rm PDF}$ the PDF uncertainties obtained with each set, and with $\Delta_{\rm PDF}$ the shift between the central value obtained and the central value used when generating pseudo-data.

NNPDF2.1		CT10		MSTW08	
$\sin^2\theta_W \pm \delta_{\rm PDF}$	$\Delta_{\rm PDF}$	$\sin^2\theta_W \pm \delta_{\rm PDF}$	$\Delta_{\rm PDF}$	$\sin^2\theta_W \pm \delta_{\rm PDF}$	$\Delta_{\rm PDF}$
0.22265 ± 0.00087	0	0.22294 ± 0.00071	$+0.00029$	0.22332 ± 0.00031	$+0.00067$

Table 4.1: Results for the determination of PDF uncertainties from the invariant mass distributions in the ATLAS/CMS kinematics. We show the central value obtained from the fit in the Born approximation, the PDF uncertainties $\delta_{\rm PDF}$ and the shift $\Delta_{\rm PDF}$ from the central value to the value used in pseudo-data.

We summarize the results obtained when performing the fitting procedure described in Sect. 4.5.1 on the Born level invariant mass distribution in the LHCb kinematics in Table 4.2.

NNPDF2.1		CT10		MSTW08	
$\sin^2\theta_W \pm \delta_{\rm PDF}$	$\Delta_{\rm PDF}$	$\sin^2\theta_W \pm \delta_{\rm PDF}$	$\Delta_{\rm PDF}$	$\sin^2\theta_W \pm \delta_{\rm PDF}$	$\Delta_{\rm PDF}$
0.22267 ± 0.00016	$+0.00002$	0.22274 ± 0.00023	$+0.00009$	0.22265 ± 0.00011	0

Table 4.2: Results for the determination of PDF uncertainties from the invariant mass distributions in the LHCb kinematics. We show the central value obtained from the fit in the Born approximation, the PDF uncertainties $\delta_{\rm PDF}$ and the shift $\Delta_{\rm PDF}$ from the central value to the value used in pseudo-data.

4.6 Statistical uncertainties

After quantifying the impact of the PDF uncertainties, which are one of the main source of systematic uncertainties on the determination of $\sin^2\theta_W$, we focus on studying the impact of the statistical uncertainties on the measurement of the weak mixing angle. In this section we present the results we have obtained studying the statistical uncertainties in the measurement of $\sin^2\theta_W$.

4.6.1 General strategy

We have quantified the impact of the statistical uncertainties by using the template fitting method described in Section 4.5.1. In order to estimate the statistical uncertainty we have performed a rebinning, namely we have changed the bin size of the forward and the backward distribution histograms from which A_{FB} is calculated. In this way the statistical uncertainties do not differ significantly from one bin to another. The rebinning we have performed is not smooth because the statistics is greater next to the Z peak around 91 GeV. The rebinning has been performed with a particular care to the zone where the asymmetry changes sign, in order to avoid averaging between positive and negative regions, which would reduce the sensitivity to the weak mixing angle in the region where it is higher.

Starting from template zero of NNPDF2.1, 100 pseudo-data sets have been generated with gaussian fluctuations around the central value of each bin, with $\sigma_{\rm stat}$ given by Eq. (4.4) at a fixed luminosity $\mathcal{L}$.

Pseudo-data have been compared with templates and a χ^2 function has been constructed as in Eq. (4.6). For each pseudo-data there exists a preferred value for $\sin^2\theta_W$ which corresponds to the value that minimizes the χ^2. It is then possible to calculate the preferred value of $\sin^2\theta_W^{best}$ as

$$\sin^2\theta_W^{best} = \frac{1}{N_{\text{stat}}}\sum_{k}^{N_{\text{stat}}} \sin^2\theta_W^k, \tag{4.7}$$

and to compute the statistical uncertainty as

$$\sigma^2_{\sin^2\theta_W^{best}} = \frac{1}{N_{\text{stat}}-1}\sum_{k}^{N_{\text{stat}}} (\sin^2\theta_W^k - \sin^2\theta_W^{best})^2. \tag{4.8}$$

4.6.2 Results

In this section we show the plot we have obtained studying the statistical uncertainty and we show the numerical results obtained with the template fitting method.

Fig. 4.16 shows the Forward-Backward Asymmetry as a function of the invariant mass of the lepton pair after the rebinning, in both kinematical regions considered. We observe that the binning is finer in the central region of the plot where the statistics is greater whereas it is less fine in the outer region of the plot.

In Fig. 4.17 we show the statistical uncertainties for different integrated luminosities once the rebinning has been performed. We observe that after the rebinning the statistical uncertainties are similar from one bin to another. The statistical uncertainties are significantly smaller after the rebinning, as Fig. 4.18 shows. We have taken care not to reduce the sensitivity to the weak mixing angle with the rebinning. We show in Fig. 4.19 a comparison between the sensitivity with the asymmetric bins with the sensitivity obtained with the smooth, finer binning used to compute the PDF uncertainties, both in the ATLAS/CMS region and in the LHCb region.

We finally sum up the results obtained when performing the fitting procedure on the Born level invariant mass distribution in Table 4.3, with an integrated luminosity of 100 fb^{-1}.

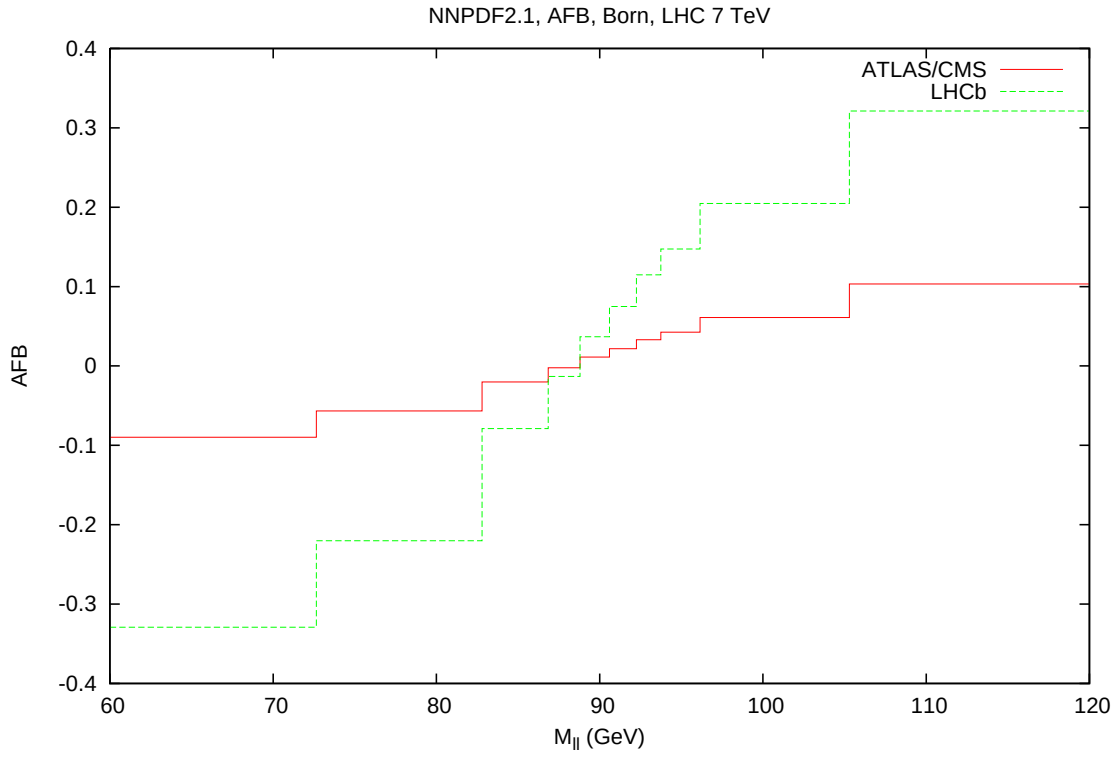

Figure 4.16: The Forward-Backward Asymmetry in the two kinematical regions after the rebinning.

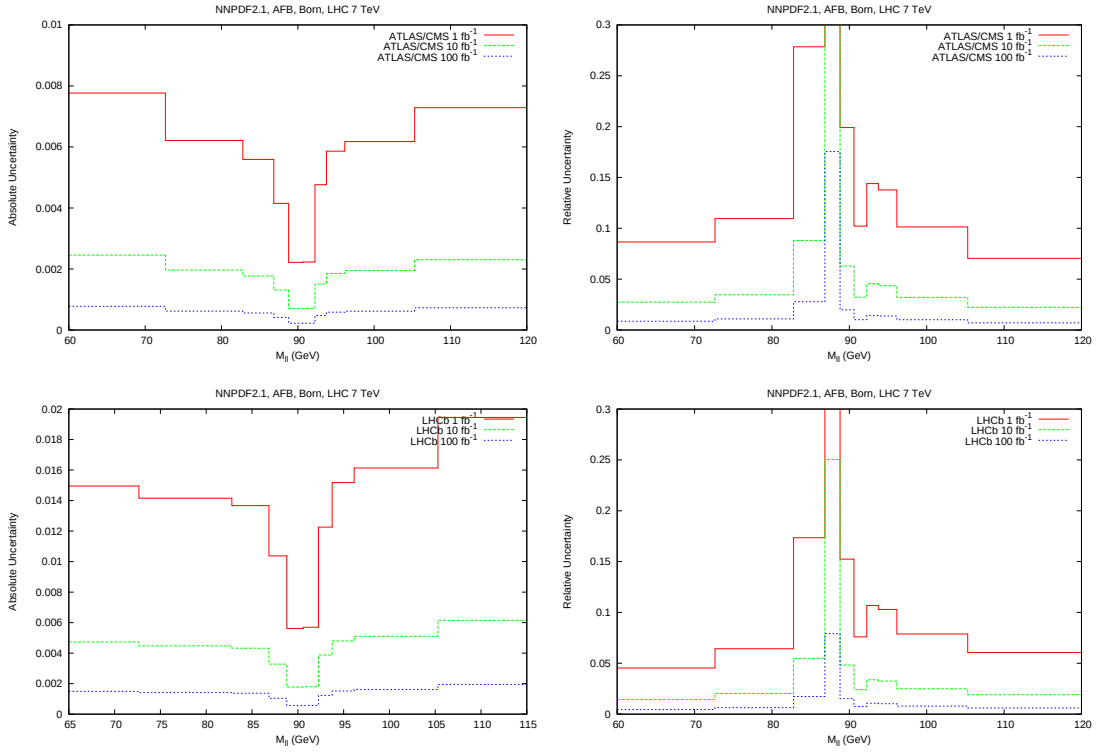

Figure 4.17: Absolute (left) and relative (right) statistical uncertainties for different integrated luminosities after the rebinning in both kinematical regions. Top: ATLAS/CMS kinematics; bottom: LHCb kinematics.

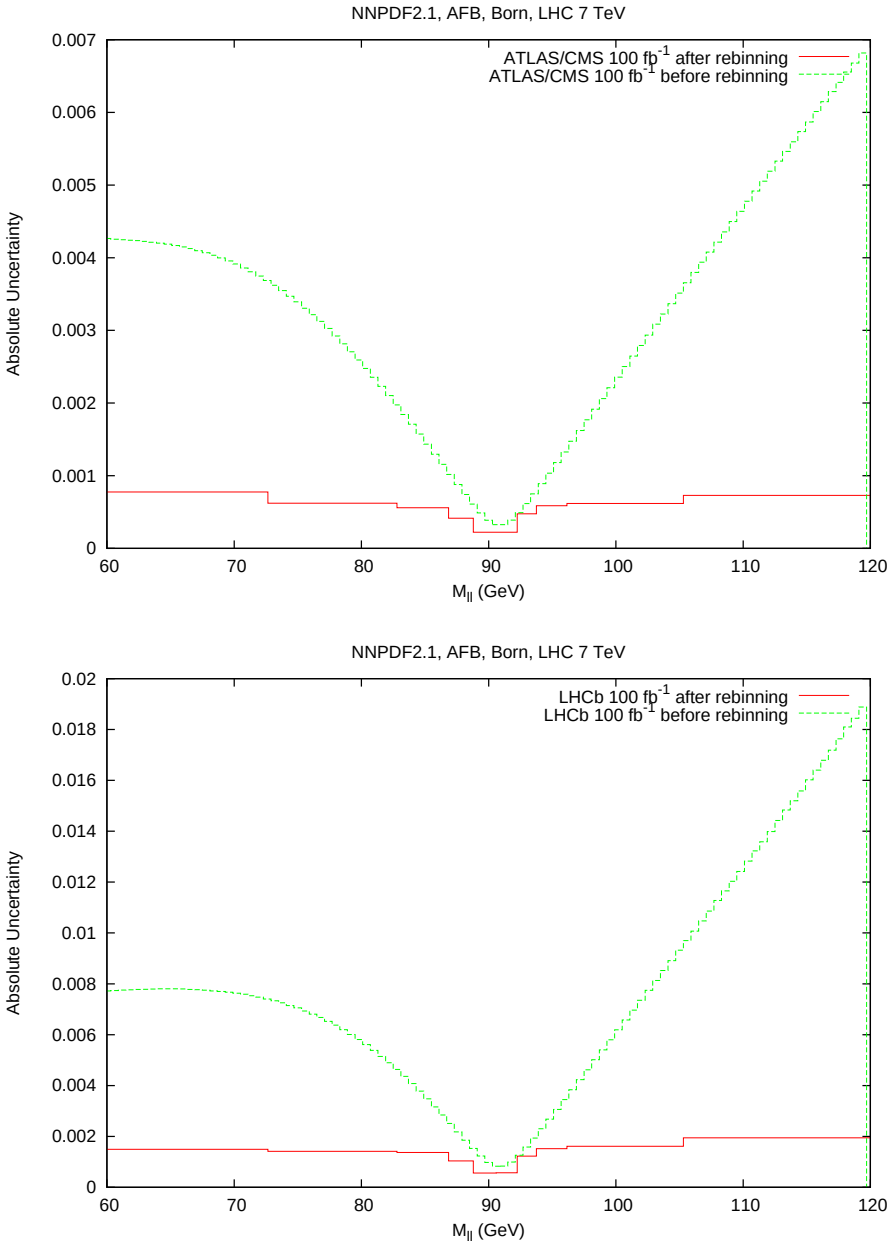

Figure 4.18: Comparison of the statistical uncertainties with $\mathcal{L} = 100$ fb^{-1} obtained with PDF from the NNPDF collaboration before and after the rebinning in both kinematical regions.

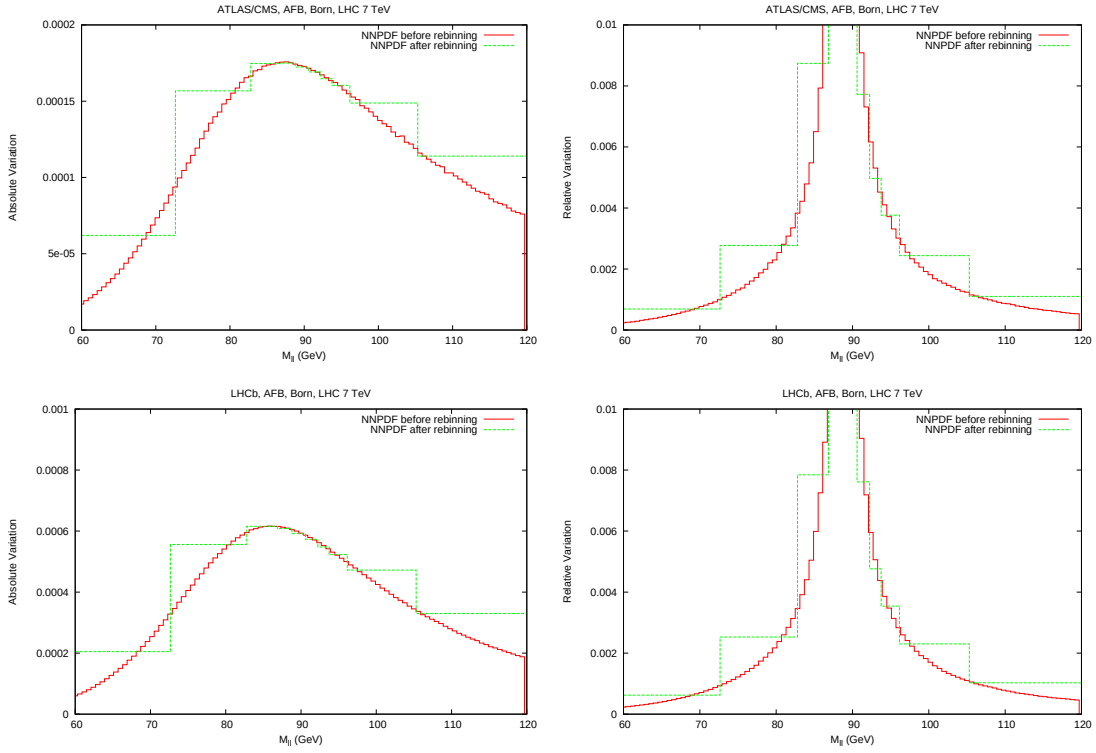

Figure 4.19: Comparison between the absolute (left) and relative (right) sensitivity to the weak mixing angle before and after the rebinning with $\delta m_W = 5$ MeV. Top: ATLAS/CMS kinematics; bottom: LHCb kinematics.

ATLAS/CMS		LHCb	
$\sin^2\theta_W \pm \delta_{\rm stat}$	$\Delta_{\rm stat}$	$\sin^2\theta_W \pm \delta_{\rm stat}$	$\Delta_{\rm stat}$
0.22266 ± 0.00015	+0.00001	0.22264 ± 0.00011	-0.00001

Table 4.3: Results for the determination of the statistical uncertainties with $\mathcal{L} = 100$ fb^{-1} from the invariant mass distributions in the LHCb kinematics. We show the central value obtained from the fit in the Born approximation, the statistical uncertainties $\delta_{\rm stat}$ and the shift $\Delta_{\rm stat}$ from the central value to the value used in pseudo-data.

4.7 Summary

In this section we summarize the results discussed in the previous sections and we compare PDF uncertainties and statistical uncertainties on the measurement of $\sin^2\theta_W$. Fig. 4.20 shows the comparison between the uncertainties computed with the PDF sets considered and the statistical uncertainty in both kinematical regions.

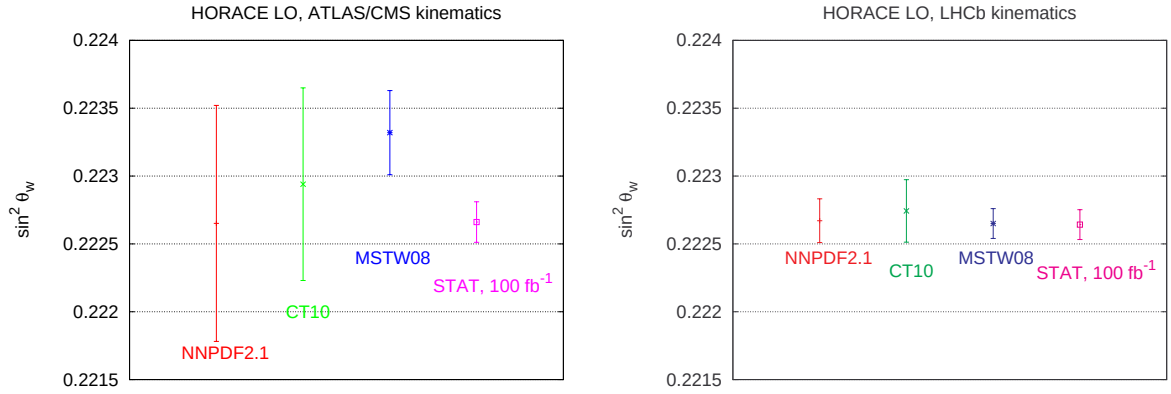

Figure 4.20: Comparison between the PDF uncertainties and the statistical uncertainty. Left: results obtained in the ATLAS/CMS kinematics; right: results obtained in the LHCb kinematics.

We found that the central values obtained with the three PDF sets differ at most by 0.0007 in the ATLAS/CMS kinematics whereas they differ by less than 0.0001 in the LHCb kinematics.

We observe that both the uncertainty due to PDF and the statistical uncertainty are greater in the ATLAS/CMS kinematics. In the ATLAS/CMS kinematics we found that the values of $\delta_{\rm PDF}$ range from 0.0003 (MSTW) to almost 0.0009 (NNPDF). However, those values are greater than the statistical uncertainty, which is less than 0.0002. In the LHCb kinematics $\delta_{\rm PDF}$ ranges from 0.0001 (MSTW) to less than 0.0003 (CT10), and is comparable with the statistical uncertainty, which is around 0.0001.

Chapter 5

Conclusions

We have studied the impact of the PDF uncertainties on the measurement of $\sin^2\theta_W$ studying the Forward-Backward Asymmetry at the LHC. We have studied the asymmetry at the Born level as a function of the invariant mass of the lepton pair in Drell-Yan neutral current events. The PDF and the statistical uncertainties on the Forward-Backward Asymmetry have been studied in two different kinematical settings. We have finally estimated the impact of the uncertainties on the measurement of the weak mixing angle by means of a template fitting method.

Our main conclusions are:

- At the Born level, the predictions for the central values obtained with different PDF sets partially agree in the ATLAS/CMS settings and they agree in the LHCb kinematics. The PDF uncertainties estimated with the different PDF sets partially agree in the ATLAS/CMS kinematics whereas they agree in the LHCb settings.
- In the ATLAS/CMS kinematics the PDF uncertainties, which are one of the main source of systematic uncertainties, dominate the statistical uncertainty. We conclude that a precise measurement of the Weinberg angle from the Forward-Backward Asymmetry in this region with the actual PDF sets is not competitive with the value of LEP Electroweak Working Group. This is mostly due to the PDF uncertainty estimated with PDFs from the NNPDF2.1 collaboration, which is the set with the most reliable uncertainties.
- At the state of art, a precise measurement of the Weinberg angle from the Forward-Backward Asymmetry is more likely to be performed at the LHCb. With the LHCb kinematical settings the uncertainties are smaller, and if one consider the envelope of the PDF uncertainties it results at the level of 2.3×10^{-4} which is comparable with the LEP Electroweak Working Group uncertainty.
- The statistical uncertainty with $\mathcal{L} = 100$ fb^{-1} is at the level of 1.5×10^{-4} in the ATLAS/CMS kinematical settings and at the level of 1.1×10^{-4} in the LHCb kinematical settings, and with this integrated luminosity it is smaller than the PDF uncertainties.

Our study shows that the PDF uncertainties at LHCb are at the level of the LEP Electroweak Working Group uncertainty. However, theoretical errors might lead to an underestimate of the impact of the PDF uncertainties. In fact, at small and large x we know only partially the theoretical behaviour. In this perspective an analytical insight might be necessary.

A detailed study of the impact of the PDF uncertainties will require a study of the QED corrections which modify the shape of the asymmetry and the sensitivity. It will be necessary to repeat this study at the NLO-QCD as the gluon initiated subprocesses may induce the uncertainties to increase. Moreover, it will be interesting to inspect the correlation between the parton distribution functions and the Forward-Backward Asymmetry since this study may provide information about the sensitivity of A_{FB} to different PDFs.

List of Tables

4.1 Results for the determination of PDF uncertainties from the invariant mass distributions in the ATLAS/CMS kinematics. 36
4.2 Results for the determination of PDF uncertainties from the invariant mass distributions in the LHCb kinematics. 36
4.3 Results for the determination of statistical uncertainties from the invariant mass distributions. 42

List of Figures

3.1 The Drell-Yan process. . . . 10
3.2 Leading contributions to the Drell-Yan process. . . . 11
3.3 Comparison of $\sin^2\theta^l_{\text{eff}}$ derived from measurement. . . . 12

4.1 Absolute and relative sensitivity of A_{FB} to the Weinberg angle in the ATLAS/CMS kinematics. . . . 19
4.2 Absolute and relative sensitivity of A_{FB} to the Weinberg angle in the LHCb kinematics. . . . 19
4.3 Comparison between the sensitivity in the two kinematical regions. . . . 19
4.4 The Forward-Backward Asymmetry with uncertainty error bands calculated with the three global PDF sets considered. . . . 22
4.5 Absolute and relative PDF uncertainties for A_{FB} obtained with the different PDF sets. . . . 23
4.6 Comparison between A_{FB} values and uncertainties obtained with the different PDF sets. . . . 24
4.7 Absolute and relative statistical uncertainties for A_{FB} with different integrated luminosities. . . . 25
4.8 Comparison of the uncertainties with the sensitivity at the electroweak mixing angle at ATLAS/CMS. . . . 26
4.9 The Forward-Backward Asymmetry with uncertainty error bands calculated with the three global PDF sets considered. . . . 28
4.10 Comparison between the Forward-Backward Asymmetry with uncertainty error bands calculated with the three global PDF sets considered in both kinematical regions. . . . 29
4.11 Absolute and relative PDF uncertainties for A_{FB} obtained with the different PDF sets. . . . 30
4.12 Comparison between A_{FB} values and uncertainties obtained with the different PDF sets. . . . 31
4.13 Absolute and relative statistical uncertainties for A_{FB} with different integrated luminosities in the LHCb kinematics. . . . 32
4.14 Comparison between the results obtained in the two kinematical regions. . . . 33
4.15 Comparison of the uncertainties with the sensitivity at the electroweak mixing angle at LHCb. . . . 34
4.16 The Forward-Backward Asymmetry in the two kinematical regions after the re-binning. . . . 38

4.17 Statistical uncertainties after the rebinning. 39
4.18 Statistical uncertainties before and after the rebinning. 40
4.19 Sensitivity after the rebinning. 41
4.20 Graphical representation of the numerical results. 42

References

[1] G. D. Coughlan, J. E. Dodd, and B. M. Gripaios, *The Ideas of Particle Physics*, Cambridge University Press, 2006.

[2] A. Das and T. Ferbel, *Introduction to Nuclear and Particle Physics*, World Scientific, 2009.

[3] M. E. Peskin and D. V. Schroeder, *An introduction to Quantum Field Theory*, Westview Press, 1995.

[4] D. H. Perkins, *Introduction to High Energy Physics*, Cambridge University Press, 2000.

[5] F. Mandl and G. Shaw, *Quantum Field Theory*, Wiley, 2010.

[6] I. J. R. Aitchison and A. J. G. Hey, *Gauge Theories*, Institutes of Physics Publishing Bristol and Philadelphia, 1993.

[7] S. Lionetti, *Determinazione simultanea della costante di accoppiamento forte α_S e della struttura partonica del nucleone*, Undergraduate Thesis, Università degli studi di Milano, 2010.

[8] S. M. Bilenky, and J. Hošec, *Glashow-Weinberg-Salam theory of electroweak interactions and the neutral currents*, Physics Report (Review Section of Physics Letters) 90, No 2, 1982.

[9] F. Abe et al, *Determination of* $\sin^2\theta_W$ *from the Forward-Backward Asymmetry* $p\bar{p} \to Z^0X \to e^+e^-X$ *interactions at* $\sqrt{s} = 1.8$ *TeV*, Phys. Rev. Lett. 67, 1502, 1991

[10] M. Dittmar, *Neutral current interference in the TeV region: The experimental sensitivity at the CERN LHC*, Physical Review D 55 1, 1997

[11] W. Hollik, U. Meier, and S. Uccirati, *The effective mixing angle* $\sin^2\theta_{eff}$ *with two-loop bosonic contributions*, Nucl. Phys. B 765, 2007.

[12] J. C. Collins and D. E. Soper, *Angular distribution of dileptons in high-energy hadron collisions*, Physical Review D, 1977.

[13] D0 Collaboration, V. Abazov, et al, *Measurement of* $\sin^2\theta^{lept}_{eff}$ *and Z-light quark couplings using the forward-backward charge asymmetry*, preprint (arXiv:1104.4590v1 [hep-ex]), 2011.

[14] C.M. Carloni Calame, G. Montagna, O. Nicrosini, and A. Vicini, *Precision electroweak calculation of the production of a high transverse-momentum lepton pair at hadron colliders*, JHEP 0710:109, 2007 (arXiv:0710.1722 [hep-ph]).

[15] F. del Aguila, Ll. Ametller, and P. Talavera, *Forward-Backward Asymmetries of Lepton Pairs in Events with a Large-Transverse-Momentum Jet at Hadron Colliders*, Phys. Rev. Lett. 89, 161802 , 2002.

[16] M. Wielers, *W and Z production: cross sections and asymmetries*, ATL-PHYS-CONF-2006-013, 2006.

[17] J. L. Rosner, *Observability of Charge Asymmetries for Lepton Pairs Produced in Present Colider Experiments*, Phys. Lett. B, 1989.

[18] U. Baur , O. Brein , W. Hollik , C. Schappacher , and D. Wackeroth, *Electroweak radiative corrections to neutral-current Drell-Yan processes at hadron colliders*, Phys. Rev. D 65, 033007, 2002, (arXiv:hep-ph/0108274v1).

[19] The ALEPH, DELPHI, L3, OPAL, SLD Collaborations, the LEP Electroweak Working Group, the SLD Electroweak and Heavy Flavour Groups, *Precision Electroweak Measurements on the Z Resonance*, Physics Report Vol 427, 2006.

[20] S. Forte, *Parton distributions at the dawn of the LHC*, Acta Physica Polonica B, Vol. 41 No 12, 2010

[21] Hung-Liang Lai, M. Guzzi, J. Huston, Zhao Li, P. M. Nadolsky, J. Pumplin, and C.-P. Yuan. *New parton distributions for collider physics*, Phys. Rev.D, 2010.

[22] A. D. Martin, W. J. Stirling, R. S. Thorne, and G. Watt. *Parton distributions for the LHC*, Eur. Phys. J. C 63, 2009.

[23] NNPDF Collaboration: R. D. Ball, L. Del Debbio, S. Forte, A. Guffanti, J. I. Latorre, A. Piccione, J. Rojo, and M. Ubiali, *A determination of parton distributions with faithful uncertainty estimation*, Nuclear Physics B 809, 2009.

[24] G. Altarelli, *Particle Physics at the LHC start*, Prog. Theor. Phys. Suppl. 187, 2011.

[25] M.W. Grunewald, *Experimental precision tests for the electroweak standard model*, Landolt-Boernstein I 21A: Elementary particles 6, 2008.

[26] G. Bozzi, J. Rojo, and A. Vicini. *The impact of PDF uncertainties on the measurement of the W boson mass at the Tevatron and the LHC*, Phys. Rev. D 83, arXiv:1104.2056 [hep-ph], 2011.